Efficient Model Compression for Bayesian Neural Networks

Diptarka Saha, Zihe Liu, Feng Liang

Abstract.

Model Compression has drawn much attention within the deep learning community recently. Compressing a dense neural network offers many advantages including lower computation cost, deployability to devices of limited storage and memories, and resistance to adversarial attacks. This may be achieved via weight pruning or fully discarding certain input features. Here we demonstrate a novel strategy to emulate principles of Bayesian model selection in a deep learning setup. Given a fully connected Bayesian neural network with spike-and-slab priors trained via a variational algorithm, we obtain the posterior inclusion probability for every node that typically gets lost. We employ these probabilities for pruning and feature selection on a host of simulated and real-world benchmark data and find evidence of better generalizability of the pruned model in all our experiments.

Keywords: Bayesian Deep learning, Spike-and-slab prior, Variational inference, Model compression, Feature selection.

1 Introduction

Neural network based pattern learning techniques have influenced modern technology like very few things before it has. One of the biggest advantages that neural network models enjoy over traditional statistical learning methods is their ability to approximate, to any degree of precision, any functional form that may be present in the inherent data generation method (Hornik, 1991). This flexibility has allowed large-scale democratization of such methods (LeCun et al., 2015; Goodfellow et al., 2016).

The flexibility or complexity of a neural network model is controlled by its architecture (i.e., the depth and/or width of each layer). Although a 'large' or over-parametrized network can approximate any data-generating function to arbitrary precision, there are several drawbacks of an over-parametrized model. First of all, over-parameterised models tend to overfit the data and degrade generalization to unseen examples (Bartoldson et al., 2020); for example, experiments in Zhang et al. (2021) have shown that it is easy to train neural networks to fit random labels and such models, of course, have generalization errors no better than random guessing. Although research has shown that over-parameterized neural networks can achieve good generalization performance due to implicit regularization imposed by training algorithms such as early stopping or stochastic gradient descent, the interplay among model complexity, regularization, and the generalization error of a large neural network model has still not been fully understood (Belkin et al., 2019; Zhang et al., 2021). Further, a large model comes at the cost of additional memory and computation effort during model training and inference (Hoefler et al., 2021). Sparse models, on the other hand, are easier to store with

© 0000 International Society for Bayesian Analysis

DOI: 0000

computational savings and are more robust against adversarial attacks (Rakin et al., 2020).

Techniques used to reduce the complexity of a neural network while retaining much or all of its predictive power are, collectively, termed as *model compression*. Systematic reviews, such as Cheng et al. (2018), categorize recent developments in model compression for deep neural networks into four broad categories: parameter pruning, low-rank factorization, transferred convolutional filters, and knowledge distillation. In this paper, we focus on *parameter pruning*, this technique entails compressing an existing, typically large and accurate, trained network by systematically removing parameters from it while keeping the accuracy unharmed. Pruning has quite a rich history (Janowsky, 1989; Mozer and Smolensky, 1988; Goh and Tan, 1994); however, it has seen an explosion of interest in the past decade. Within the framework of pruning, it is common to assign a score for relevance to each parameter; based on the scores, we then remove individual parameters (*unstructured pruning or weight pruning*). Blalock et al. (2020) offers an excellent review of the state of pruning for neural networks.

We will employ a Bayesian approach to neural network pruning – it not only provides valid uncertainty estimates but also allows for the concurrent estimation of regression coefficients and complexity parameters. As Rockova et al. (2012) puts it, Bayesian regularization falls within the versatile framework of Bayesian hierarchical models. In particular, we formulate the problem of parameter pruning as a special case of Bayesian variable selection (O'Hara and Sillanpää, 2009; Clyde and George, 2004). We consider structured pruning, removing a weight/neuron (weight/node pruning) or an entire feature (feature reduction/variable pruning). In the Bayesian framework, the problem of parameter pruning may be viewed as a special case of variable selection. There have been many notable works on the theory and application of feature selections in a BNN recently (Faming Liang and Zhou, 2018; Dinh and Ho, 2020; Li et al., 2015; Liu, 2021). In the broader Bayesian literature, the gold standard for Bayesian variable selection revolves around the use of spike-and-slab priors (Mitchell and Beauchamp, 1988; George and McCulloch, 1993; Smith and Kohn, 1996; Clyde et al., 1996; George and McCulloch, 1997; Ishwaran and Rao, 2005). This is convenient as it can seamlessly integrate model averaging and variable selection within a single estimation process. In this strategy, we rely on an auxiliary indicator variable Z, which denotes if the slab or spike part of the prior is dominant to infer whether the feature is included in the model or not, respectively. Thus, direct inference on the distribution of Z is imperative.

Bayesian methods have been used in neural networks (Neal, 1995; MacKay, 1992). Bayesian neural networks (BNNs) present distinct advantages over regular neural networks by offering a natural mean for uncertainty quantification and model interpretation. In practice, however, BNNs suffer from high computational costs as exact Bayesian inference on the weights of a neural network is intractable and decent approximations are resource intensive. These computational challenges further exacerbate when dealing with discrete quantities of interest, such as Z when using the spike-and-slab prior. The main contribution of our work is an efficient algorithm that learns not just a Bayesian neural network's weights but also its topology directly by approximating the posterior of the inclusion variables.

Before diving into the main content of our paper, we first briefly outline the distinctions between our work and that of two relevant papers.

- The strategy of using inclusion probabilities for regularisation purposes has been the cornerstone of the *dropout* technique (Srivastava et al., 2014). However, there are two key differences between our method and these works: in dropout, (i) the sparsity is layerwise and doesn't apply to weights individually, and (ii) more importantly, the sparsity is fixed beforehand and not learned from the data itself. Thus our work may be viewed as an *adaptive* version of dropout In fact, Gal (2016) has argued that using a spike-and-slab prior may be seen as a particular form of dropout training; he further mentioned that typical dropout training is non-adaptive and hence a grid search may be required. Here we can reach the same goal of learning the topology of the network directly.
- Another work that we feel is closely related to ours is the variational approximation technique Bayes by Backprop from Blundell et al. (2015). They do accommodate spike-and-slab priors on the weights but avoid the computational challenges on the posterior by using mean field Gaussian variational distribution this camouflages the potential sparsity in the data. We remove this restriction in this work to learn and leverage this sparsity.

The remainder of this paper is arranged as follows. Section 2 discusses the background: we lay down the setup in Section 2.1, discuss the variational approach to BNN training in Section 2.2, provide a brief review of pruning techniques in BNNs in Section 2.3, and finally in Section 2.4, collate the gap in the literature and discuss how we intend to address it. Section 3 provides the main contribution that we combine into one algorithm for training a sparse BNN and a feature relevance detection strategy defined. Finally, Section 4 discusses all the experiments. We conclude the paper with a discussion and future prospects in Section 5.

2 Background

2.1 Setup

Given a dataset \mathcal{D} consisting n independent observations of $\mathbf{x} = (x_1, \dots, x_p)$ and target y, we are interested in learning their relationship so that given a new data-point x^* we are able to provide an accurate prediction y^* . For a neural network with L hidden layers, the estimated model has the following form:

$$\hat{y} = f_{\mathbf{W}}(\mathbf{x}) = \sigma_L \cdots \sigma_2 (\sigma_1 (\mathbf{x}^T w_1 + b_1)^T w_2 + b_2) \cdots). \tag{2.1}$$

where $\{\sigma_j\}_1^L$ are (typically non-linear) activation functions specified by the user. For example, the ReLU (rectified linear unit) activation function is defined as: $\sigma(z) = \max(z,0)$. The complexity of the model (2.1) can be further increased by increasing the number of layers and/or nodes in each layer. The goal then is to train the network

such that some loss is minimized; for example, for regression tasks, we might be interested to minimise the euclidean loss between actual and predicted values, while for classification tasks we may be interested in minimizing the cross-entropy loss.

Although methods like these have been successful in complicated pattern recognition tasks, they have remained statistical black boxes lacking critical information needed for inference such as uncertainties associated with the predictions. Bayesian methods offer a natural way to reason about uncertainty in predictions and can provide insight into how these decisions are made. To do this, a distribution is placed over the network parameters and the resulting network is then termed a Bayesian Neural Network (BNN).

Formally, consider a BNN with L layers and n_l nodes in each layer $l \in \{1, ..., L\}$. Let $\mathbf{W} = \{w_j, b_j\}_1^L$ denote the corresponding parameters where w_j denotes the $n_{l-1} \times n_l$ weight matrix, b_j denotes the $n_l \times 1$ bias vector, and $n_0 = p$, the input feature dimension. Let $\pi(\cdot)$ denote the prior on \mathbf{W} . The objective, then, will be to compute the resulting posterior distribution:

$$\pi(\mathbf{W}|\mathcal{D}) = \frac{\pi(\mathbf{W})p(\mathcal{D}|\mathbf{W})}{p(\mathcal{D})}.$$
 (2.2)

Neal (1995) popularised such a setup with Gaussian priors for his networks. In the past decade, authors have employed several priors that help their use-case including mixed Gaussian (Blundell et al., 2015), Horseshoe (Louizos et al., 2017), etc.

Leveraging this distribution, we can predict output for a new input point x^* by integrating:

$$p(y^*|x^*, \mathcal{D}) = \int p(y^*|x^*, w)p(w|\mathcal{D})dw.$$

Note, since the output is an entire distribution and not just one value, we can easily proceed to investigate any statistic we are interested in, including the mean and uncertainty estimates among others. This advantage has promoted BNNs to prominence as the explainability of artificial intelligence has emerged to be of paramount interest, especially security-critical applications (Bykov et al., 2021).

2.2 Approximate Posterior via Variational Inference

Baring certain ideal cases of conjugate prior, the posterior (2.2) is not analytically tractable. Thus the problem of numerically approximating the posterior is imperative. Some early notable works include Neal (1995)'s hybrid Monte Carlo or Hamiltonian Monte Carlo; MacKay (1992)'s Laplace method; and Hinton and van Camp (1993)'s MDL-based approach under a variational inference interpretation, which was further generalized by Barber and Bishop (1998). Please see Goan and Fookes (2020) for a thorough review.

In this work, we focus on variational inference (VI). VI frames marginalization required during Bayesian inference as an optimization problem. This is achieved by assuming the form of the posterior distribution and performing optimization to find the assumed density closest to the true posterior. This assumption simplifies computation and provides some level of tractability.

The assumed variational distribution $q_{\theta}(\cdot)$ is a suitable density over the set of parameters \mathbf{W} , which is restricted to a certain family of distributions parameterized by θ . The parameters for this variational distribution are then adjusted to reduce the dissimilarity between the variational distribution and the true posterior. The dissimilarity is often measured by their KL divergence:

$$KL(q_{\theta}(\mathbf{W})||\pi(\mathbf{W}|\mathcal{D})) = \int q_{\theta}(\mathbf{W}) \log \frac{q_{\theta}(\mathbf{W})}{\pi(\mathbf{W}|\mathcal{D})} d\mathbf{W}$$

$$= \int q_{\theta}(\mathbf{W}) \log \frac{q_{\theta}(\mathbf{W})}{\pi(\mathbf{W})p(\mathcal{D}|\mathbf{W})/p(\mathcal{D})} d\mathbf{W}$$

$$= KL(q_{\theta}(\mathbf{W})||\pi(\mathbf{W})) - \mathbb{E}_{q_{\theta}(\mathbf{W})} \log p(\mathcal{D}|\mathbf{W}) + \log p(\mathcal{D}).$$

Note that the last term is independent of θ . Thus, finding the optimal variation parameter is equivalent to maximizing the following objective function:

$$-\mathrm{KL}(q_{\theta}(\mathbf{W})||\pi(\mathbf{W})) + \mathbb{E}_{q_{\theta}(\mathbf{W})} \log p(\mathcal{D}|\mathbf{W}). \tag{2.3}$$

This objective function, often termed the Evidence Lower BOund (ELBO), contains two antagonistic terms: a prior-dependent part and a data-dependent part. Thus finding an optimal variational posterior $q_{\theta}(\cdot)$ can be thought of as finding the balance between the complexity of the data \mathcal{D} and simplicity of the prior $\pi(\cdot)$.

Gradient descent is often used to optimize (2.3). However, computing the gradient of the second term is often analytically impossible and computationally challenging. To alleviate the issue, Williams (1992) uses the so-called log-derivative trick, which leverages the differential rule, $\nabla_{\theta}p_{\theta}(x) = p_{\theta}(x)\nabla_{\theta}\log p_{\theta}(x)$, for any density p parameterised by θ . This trick is easy to implement and often quite useful, especially if the density in question belongs to the exponential family. However, the Monte Carlo estimates of the gradients computed using such methods suffer from high variance, which necessitates higher resources for computation. Alternatively, Blundell et al. (2015) has outlined a general pragmatic approach to optimize the variational parameters, which relies heavily on the reparametrization trick (Kingma and Welling, 2014). This method yields low variance but is restricted only to the continuous family of distributions. More details on this technique will be discussed in Section 3.

2.3 Prior Work on Bayesian Pruning

The earliest idea of pruning a neural network was introduced by LeCun et al. (1990). Han et al. (2015) have applied the same idea to modern architectures. Simple heuristic methods removing weights of small magnitude have also been employed with great compression ratio but without much theoretical justification (Ström, 1997; Collins and Kohli, 2014). The issue has also been targeted from a Bayesian perspective in works such as Neal (1995), MacKay (1992), etc. While theoretically sound, these results lack scalability due to the difficulty of obtaining or estimating the posterior.

Perhaps, in the past decade, the most popular and empirically effective method for regularising a neural network has been the *Dropout* method (Srivastava et al., 2014). In

this method, we add multiplicative noise to the input of each layer of the neural network which makes the weights less likely to overfit (Kingma et al., 2015). In their seminal work, Gal and Ghahramani (2016) added Bayesian justification for this approach by establishing it as an approximation to a Gaussian Process. Despite its success, initial versions of dropout had some major drawbacks: working with binary errors is expensive; but more importantly, the sparsity parameters (dropout rates) are fixed and not learned from the data. Further to avoid potential complexity the rates were also shared across layers, which masks the sparsity of individual weights and nodes.

In Gaussian Dropout, Wang and Manning (2013) alleviated the first issue by successfully showing that one can reap all the benefits of the dropout by using an appropriately selected Gaussian noise instead of a binary one. In Variational Dropout, Kingma et al. (2015) re-imagined the Gaussian Dropout as a variational approximation procedure with Jeffrey's prior $\pi(w) \propto \frac{1}{w}$ on the weights and the variational posterior $q(w) \sim N(\theta, \alpha\theta^2)$. Manipulating the variational objective function will allow us to learn the individual dropout rates for each layer, node, or weight – facilitating a sparse solution. The idea has been further modified and verified empirically in Molchanov et al. (2017). Extensions of similar ideas have been demonstrated in Louizos et al. (2017), where the authors used the same variational posterior as in Kingma et al. (2015), but a scaled mixture of Gaussian prior to achieve Bayesian compression.

2.4 Motivation

The spike-and-slab prior remains the gold standard for a Bayesian relevance determination of a parameter. However, approaches for pruning a BNN have avoided inferring the inclusion probability of any weight due to the associated complexity in estimating the gradient. The difficulties stem from the fact that the reparameterization trick becomes inapplicable if the quantities of interest have discrete distribution simply due to the fact that the objective function thereof ceases to be differentiable and hence estimation of the gradient is impossible. This presents a conundrum – in order to induce sparsity we must infer about *inclusion variables* that will take binary (discrete) values. Algorithms recruiting the reparameterization trick, such as *Bayes by Backprop* from Blundell et al. (2015), will fail to do so.

In their original work, Blundell et al. (2015) has only used mean field Gaussian posterior but demonstrated a possible strategy for pruning by looking at the signal-to-noise ratio of each weight. While the empirical utility of such rule-of-thumb techniques is well-established, they do not provide a principled way to estimate the posterior inclusion probability of any weight. In Molchanov et al. (2017) and extensions thereof, authors explicitly use a continuous mixture of Gaussian priors continuous instead of discrete spike-and-slab prior to reduce computational expense. Investigations into the application of the reparameterization trick for discrete parameters are still nascent at this time. Some approaches include the use of techniques such as marginalization (Tokui and sato, 2016), Gaussian approximation (Shayer et al., 2018), and the Straight-through estimator (Courbariaux et al., 2016; ?; Rastegari et al., 2016).

In this work, we employ the spike-and-slab prior to the weights. For the posterior,

unlike previous works, we assume multiplicative mean field Bernoulli (for inclusion probabilities) and Gaussian (for weight sizes) distributions. The aforementioned issues are bypassed by leveraging nice relationships among the concerned parameters arising in this particular case. By estimating not just the Gaussian but also the Bernoulli parameters, we can learn the optimal model topology with probabilistic guarantees. We leverage these probabilities to generate strategies that facilitate weight pruning and feature pruning.

3 Method

3.1 A New VI Objective Function

The architecture of any neural network is heuristic at best; thus redundancies are likely to prevail. In Bayesian literature, a common weapon to identify and eliminate such redundancies is the sparsity-inducing spike-and-slab prior. We will assume the same here for all weights and biases with a unique sparsity-inducing variable Z_i for each parameter. The spike-and-slab prior can be written as follows:

$$\pi(\mathbf{W}, \mathbf{Z}) = \prod_{\mathbf{W}, \mathbf{Z}} \left[\pi \cdot \mathcal{N}(w_i; 0, \tau_1^2) \right]^{Z_i} \cdot \left[(1 - \pi) \cdot \mathcal{N}(w_i; 0, \tau_0^2) \right]^{(1 - Z_i)}$$
(3.1)

where $\tau_0^2 < \tau_1^2$. Note that if we integrate over the binary latent variables **Z**, we retrieve the marginal prior distribution on weights used in Blundell et al. (2015):

$$\pi(\mathbf{W}) = \prod_{\mathbf{W}} \left[\pi \cdot \mathcal{N}(w_i; 0, \tau_1^2) + (1 - \pi) \cdot \mathcal{N}(w_i; 0, \tau_0^2) \right].$$

The objective, then, will be to compute the resultant posterior distribution

$$\pi(\mathbf{W}, \mathbf{Z}|\mathcal{D}) \propto \pi(\mathbf{W}, \mathbf{Z})p(\mathcal{D}|\mathbf{W}).$$
 (3.2)

As mentioned in Section 2.4, the existing scalable methods exclude discrete variables such as **Z**. We intend to bridge this gap by assuming a separate variational distribution on the latent binary inclusion variable along with the network weights:

$$q_{\mathbf{p}}(\mathbf{Z}) = \prod_{\mathbf{Z}} Bern(Z_i; p_i), \quad q_{\theta}(\mathbf{W}) = \prod_{\mathbf{W}} \mathcal{N}(w_i; m_i, \sigma_i^2),$$
 (3.3)

where $\theta = \{m_i, \sigma_i^2\}_{i=1}^M$ and $\mathbf{p} = \{p_i\}_{i=1}^M$ denote all the variational parameters associated with \mathbf{W} and \mathbf{Z} , respectively. We may refer to θ as 'weight parameters' and \mathbf{p} as 'sparsity parameters'.

Our variational objective function then becomes

$$\mathcal{J}(\theta, \mathbf{p}) = -\mathbb{E}_{q_{\theta}(\mathbf{W})} \mathbb{E}_{q_{\mathbf{p}}(\mathbf{Z})} \log \frac{p(\mathcal{D}|\mathbf{W}) \cdot \pi(\mathbf{W}, \mathbf{Z})}{q_{\theta}(\mathbf{W}) \cdot q_{\mathbf{p}}(\mathbf{Z})}.$$
(3.4)

This objective function explicitly optimizes the distribution of the inclusion variable while making it customizable for each weight individually and providing the optimal sparsity for each weight. This constitutes a stark difference from *Dropout* and *Bayes by Backprop*, which is the core of our work.

To compute the gradient of (3.4), we use the reparametrization trick (Kingma and Welling, 2014), which is, in essence, very similar to pivoting technique (Casella and Berger, 2002) used in classical statistics. This trick hinges on the fact that a random variable may be represented as a combination of a deterministic and a differentiable expression. For example, with $\theta = \{\mu, \sigma^2\}$, if $\omega \sim N(\mu, \sigma^2)$ and $\epsilon \sim N(0, 1)$, then

$$\omega = g(\theta, \epsilon) = \mu + \sigma \cdot \epsilon. \tag{3.5}$$

This allows us to make the expectations in (3.4) free of parameters θ by rewriting them in terms of this simpler, differentiable random variable ϵ .

Complications arise in the optimization process with the discrete random variables Z_i , as they cannot be reparametrised as a differentiable function of a continuous random variable. Thus, the objective function ceases to be differentiable. However, the following result notes that the dependence on Z_i 's variational parameter p_i is isolated only to a non-stochastic penalty term. Thus, we can bypass the computational challenges and will still be able to use the reparametrization trick.

Proposition 3.1. The objective function (3.4) can be alternatively expressed as

$$\mathcal{J}(\theta, \mathbf{p}) = -\mathbb{E}_{q_{\theta}(\mathbf{W})} \log p(\mathcal{D}|\mathbf{W}) + \sum_{i} \mathcal{R}(\theta_{i}, p_{i})$$
(3.6)

up to a constant, where

$$\mathcal{R}(\theta_i, p_i) = p_i \cdot \left[\frac{m_i^2 + \sigma_i^2}{2\tau_1^2} + \log \frac{\tau_1 p_i}{\sigma_i \pi} \right] + (1 - p_i) \cdot \left[\frac{m_i^2 + \sigma_i^2}{2\tau_0^2} + \log \frac{\tau_0 (1 - p_i)}{\sigma_i (1 - \pi)} \right]. \quad (3.7)$$

Note that p_i 's, the variational parameters associated with the discrete latent variables Z_i 's, appear only in the second term of the objective function (3.6). As demonstrated in the following result, for any given set of weight parameter values $\theta_i = (m_i, \sigma_i^2)$, the optimal value of the sparsity parameter p_i can be expressed as a closed-form function of θ_i .

Proposition 3.2. For any set of values of the weight parameters (m_i, σ_i^2) , the optimal value of the sparsity parameter p_i^* satisfies the following equality:

$$p_i^*(\theta_i) = \frac{1}{1 + \exp\{A_i - B_i\}},\tag{3.8}$$

where

$$A_i = \frac{m_i^2 + \sigma_i^2}{2\tau_1^2} + \log \frac{\tau_1}{\pi}, \quad B_i = \frac{m_i^2 + \sigma_i^2}{2\tau_0^2} + \log \frac{\tau_0}{1 - \pi}.$$

The proofs of these results may be found in the supplementary material.

3.2 Algorithm to Optimise J

The above two results, Proposition 3.1 and Proposition 3.2, suggest a coordinate descent algorithm for the optimization of (3.4): at every iteration, given the sparsity parameters \mathbf{p} , update θ via gradient descent; then given the weight parameters θ , update \mathbf{p} via the closed-form function (3.8).

Optimization over θ can be done using the reparametrization trick. First, let $\mathcal{R}(\theta_i)$ denote $\mathcal{R}(\theta_i, p_i)$, which is a function of θ_i only when **p** is given. Then write the objective function (3.6) as

$$\mathcal{J}(\theta) = \mathbb{E}_{q_{\theta}(\mathbf{W})} \left[-\log p(\mathcal{D}|\mathbf{W}) + \sum_{i} \mathcal{R}(\theta_{i}) \right]. \tag{3.9}$$

Define $f(\theta, \mathbf{W}) = -\log p(\mathcal{D}|\mathbf{W}) + \sum_{i} \mathcal{R}(\theta_{i})$. Following (3.5), we can write for this differentiable function f,

$$\mathbb{E}_{q_{\theta}(\mathbf{W})}[f(\theta, \mathbf{W})] = \mathbb{E}_{\phi(\epsilon)}[f(\theta, g(\theta, \epsilon))] = \int f(\theta, g(\theta, \epsilon))\phi(\epsilon)d\epsilon,$$

where $\mathbf{W} = g(\theta, \boldsymbol{\epsilon})$ is the multivariate version of (3.5) and $\phi(\cdot)$ denotes the standard multivariate Gaussian density function. Since $\boldsymbol{\epsilon}$ is free of θ , the integral and the gradient operators can be interchanged:

$$\nabla_{\theta} \mathbb{E}_{q_{\theta}(\mathbf{W})} [f(\theta, \mathbf{W})] = \nabla_{\theta} \mathbb{E}_{\phi(\epsilon)} [f(\theta, g(\theta, \epsilon))] = \mathbb{E}_{\phi(\epsilon)} [\nabla_{\theta} f(\theta, g(\theta, \epsilon))]. \tag{3.10}$$

This gradient can be numerically approximated. We can sample L many i.i.d. samples of ϵ from standard multivariate Gaussian distribution and find the Monte Carlo estimate:

$$\mathbb{E}_{\phi(\epsilon)}[\nabla_{\theta} f(\theta, g(\theta, \epsilon))] \approx \frac{1}{L} \sum_{l=1}^{L} \nabla_{\theta} f(\theta, g(\theta, \epsilon^{(l)})). \tag{3.11}$$

Following (3.10) and (3.11), the gradient for the objective function may be calculated and approximated as

$$\frac{\partial}{\partial \theta} \mathcal{J}(\theta) = \mathbb{E}_{\phi(\epsilon)} \left[\frac{\partial}{\partial \theta} f(\theta, \mathbf{W}) \right] \approx \frac{1}{L} \sum_{l=1}^{L} \left[\frac{\partial f}{\partial \mathbf{W}} \frac{\partial \mathbf{W}}{\partial \theta} + \frac{\partial f}{\partial \theta} \right]. \tag{3.12}$$

This optimization process is summarised in the following automated algorithm. Here, the variational parameters are $\theta = \{m, \rho\}$ and $\sigma = \log(1 + e^{\rho})$; this is to make sure we have positive variance. The output of the algorithm is the mean, and variance of the final Gaussian distribution for each weight, and its probability of coming from the slab component.

Algorithm 1 Sparse BNN Approximation

```
1: procedure \operatorname{sBNN}(\theta, \mathcal{D}, \alpha)

2: repeat

3: Sample: \epsilon \sim N(\mathbf{0}, \mathbf{I})

4: Let \theta = (\mathbf{m}, \boldsymbol{\rho})

5: Set \mathbf{W} = \mathbf{m} + \log(1 + \exp(\boldsymbol{\rho})) \odot \epsilon

6: Compute f(\mathbf{W}, \theta, p) = -\log p(\mathcal{D}|\mathbf{W}) + \mathcal{R}(\theta, p)

7: Compute the gradients using reparametrization technique
```

$$\nabla_{m} = \frac{\partial f}{\partial \mathbf{W}} + \frac{\partial f}{\partial m}$$
$$\nabla_{\rho} = \frac{\partial f}{\partial \mathbf{W}} \frac{\epsilon}{1 + \exp(-\rho)} + \frac{\partial f}{\partial \rho}$$

8: **Update the weight parameters** using gradient descent

$$m \longleftarrow m - \alpha \nabla_m$$
$$\rho \longleftarrow \rho - \alpha \nabla_\rho$$

9: Update the sparsity parameter using (3.8)

$$\begin{split} \sigma &\longleftarrow \log(1 + \exp(\rho)) \\ A &\longleftarrow \frac{m + \sigma^2}{2\tau_1^2} + \log \frac{\tau_1}{\pi} \\ B &\longleftarrow \frac{m^2 + \sigma^2}{2\tau_0^2} + \log \frac{\tau_0}{1 - \pi} \\ p &\longleftarrow \frac{1}{1 + \exp\{A - B\}} \end{split}$$

10: **until** Convergence

11: end procedure

12: **Output**: $\{m_i, \sigma_i^2, p_i\}$ for each weight $w \in \mathbf{W}$

3.3 Comparing Objective Functions

Incorporating the sparsity parameter indirectly into the objective function creates some compelling parallel with the *Bayes by Backprop* method from Blundell et al. (2015). In this section, we compare the objective function we are solving, denoted by \mathcal{J} defined in (3.9), to that from Blundell et al. (2015), denoted by \mathcal{J}_B :

$$\mathcal{J}(\theta) = \mathbb{E}_{q_{\theta}(\mathbf{W})} \Big[-\log p(\mathcal{D}|\mathbf{W}) + \sum_{i} \mathcal{R}(\theta_{i}) \Big]$$

$$\mathcal{J}_{B}(\tilde{\theta}) = \mathbb{E}_{q_{\tilde{\theta}}(\mathbf{W})} \Big[-\log p(\mathcal{D}|\mathbf{W}) - \log \frac{\pi(\mathbf{W})}{q_{\tilde{\theta}}(\mathbf{W})} \Big],$$

where two variational distributions $q_{\tilde{\theta}}$ and q_{θ} on **W** take the same form as defined in (3.3).

In particular, we compare their gradients. Let's drop the index without loss of generality and only compare for one weight W. Since the first term is the same in both these functions, we compare the second term, which is

$$f(W, m) = -\log \pi(W) + \log q(W|m)$$

in J_B and $\mathcal{R}(\theta)$ in our objective function J. See the Supplementary Material for detailed derivation.

First, let us compare the gradient with respect to the mean parameter m. An MCMC Estimate of $\nabla_m f$ in Blundell et al. (2015) is given by

$$\hat{\nabla}_m f = \frac{\hat{W}}{\tau_1^2} \frac{\pi_1(\hat{W})}{\pi(\hat{W})} + \frac{\hat{W}}{\tau_0^2} \frac{\pi_0(\hat{W})}{\pi(\hat{W})}$$
(3.13)

where $\hat{W} = m + \sigma \hat{\epsilon}$ is a sample from $N(m, \sigma^2)$. On the other hand, the gradient of $\mathcal{R}(\theta)$ in our approach is

$$\nabla_m \mathcal{R}(\theta) = \frac{m}{\tau_1^2} p + \frac{m}{\tau_0^2} (1 - p) = \frac{m}{\tau_1^2} \frac{\pi_1(m)}{\pi(m)} + \frac{m}{\tau_0^2} \frac{\pi_0(m)}{\pi(m)}.$$
 (3.14)

These two gradients are directly comparable, notice $\frac{\pi_1(W)}{\pi(W)} = \mathbb{E}(Z|W)$ and $p = \mathbb{E}_{q(Z)}Z$. Since we have explicitly obtained distribution for Z, we can use its expectation directly. However, in Blundell et al. (2015)'s case they have to use its conditional expectation (and estimates thereof) given a weight value since Z doesn't have a direct distribution. Similarly, our objective function substitutes the variational mean $m\mathbb{E}_{q(W)}W$ of

For the variance parameter σ^2 similar comparisons exist. In our case, the gradient is

$$\nabla_{\sigma^2} \mathcal{R}(\theta) = \frac{1}{2} \left(\frac{1}{\tau_1^2} p + \frac{1}{\tau_0^2} (1 - p) - \frac{1}{\sigma^2} \right), \tag{3.15}$$

while an MCMC estimate of the gradient in Blundell et al. (2015) is given by

W, instead of the whole random variable.

$$\hat{\nabla}_{\sigma^2} f = \frac{1}{2} \left(\frac{m}{\sigma} \hat{\epsilon} + \hat{\epsilon}^2 \right) \left(\frac{1}{\tau_1^2} \frac{\pi_1(\hat{W})}{\pi(\hat{W})} + \frac{1}{\tau_0^2} \frac{\pi_0(\hat{W})}{\pi(\hat{W})} - \frac{1}{\sigma^2} \right) + \frac{1}{2\sigma^2} \left(\hat{\epsilon}^2 - 1 + \frac{m}{\sigma} \hat{\epsilon} \right)$$
(3.16)

From the previous discussion regarding the mean parameter, it is clear that the middle term in (3.16) is analogous to the whole gradient in (3.15). The other two terms are random, and in Blundell et al. (2015)'s algorithm, these are estimated via MCMC. However, these terms also have the following nice properties that help us see the comparison through:

$$\mathbb{E}\left(\frac{m}{\sigma}\hat{\epsilon} + \hat{\epsilon}^2\right) = 1, \quad \mathbb{E}\left((\hat{\epsilon}^2 - 1) + \frac{m}{\sigma}\hat{\epsilon}\right) = 0.$$

In summary, we observe that the gradients have a very similar form in both, while certain quantities of interests have different but analogous estimates. Most importantly, for the distribution of Z, we use the exact expectation given by p_i from (3.4), while Bayes by Backprop uses its conditional expectation given a random sample of the weight. This highlights the core difference, and showcases how even though the ideas are along similar lines, we can leverage explicitly the variational distribution of the sparsity parameter that we have employed.

3.4 Remarks on the Final Solution

Finally, let us discuss some repercussions of using this sparsity parameter learned through our algorithm. To do so, first, we observe, the final solution as described in (3.8) can also be written as

$$2\left(\operatorname{logit}(p_i) - \operatorname{logit}(\pi_i)\right) = \left(m_i^2 + \sigma_i^2\right) \left(\frac{1}{\tau_0^2} - \frac{1}{\tau_1^2}\right) - \log\frac{\tau_1^2}{\tau_0^2}.$$
 (3.17)

Using this form, we can now remark on some interesting characteristics of our estimate of the inclusion probability.

Remark 1. For any given prior variances τ_1^2 and τ_0^2 , p_i is a monotonically increasing function of $m_i^2 + \sigma_i^2$.

This is a desirable property. A larger magnitude of the second moment indicates that the slab component is likely to be dominant, and thus p should be higher. We can then prune off weights with low-second moments. Note, this is somewhat different from pruning based on signal-to-noise ratio m_i/σ_i as originally prescribed in Blundell et al. (2015). This property also indicates: $p \to 1$ when $m_i^2 + \sigma_i^2 \to \infty$.

Remark 2. As
$$\frac{\tau_1^2}{\tau_0^2} \to 1$$
, we have $\frac{p}{\pi} \to 1$.

This is again intuitive. If we treat both our slab and spike components similarly, the posterior will look very similar to the prior.

Remark 3. If we let $\tau_1^2 \to \infty$ while keeping all else fixed, we have $p \to 0$.

This is an interesting result; there may exist some pathological choice of prior (i.e. very large τ_1) due to which no value for m,σ can indicate that the weight was coming from the slab component. This is counterintuitive, since - in its essence, our work is close to testing the significance of m - we should expect a higher value m to recommend a higher value of p. Indeed, we reckon this is a specific case of Lindley's paradox (Lindley, 1957). This can also be extended by taking $\tau_0^2 \to 0$ and keeping all else fixed, in which case, $p \to 1$.

3.5 Quantifying Feature importance

We consolidate the individual weight influences, denoted by $\{p_i\}$, to estimate the importance of any node at any layer. This strategy is particularly useful for determining feature importance, as features correspond to the nodes in the first layer. We employ the 'connection weights' method as proposed by Olden et al. (2004), where we compute the multiplicative path probability for each path that begins with a specific feature and ends at the target, and then we average these path probabilities.

Formally, consider an L-layer Bayesian Neural Network (BNN), where each weight has an associated inclusion probability p. Let $P^{(l)} \in \mathbb{R}^{n_l \times n_{l-1}}$ represent the node influence matrix between the l-th and (l-1)-st layers, where $[P^{(l)}]_{ij}$ is the inclusion probability for the weight connecting the i-th node in layer l to the j-th node in layer (l-1). Additionally, define $n_0 = p$ and $n_{L+1} = 1$. The feature importance for the j-th input feature can then be defined as:

$$\psi_j = \left[\frac{1}{\prod_{i=1}^L n_i} \left(P^{(L+1)} P^{(L)} \cdots P^{(1)} \right)^T \right]_j.$$
 (3.18)

However, note that the estimated feature relevance values may become very small in practice. This is due to the fact that ψ_j is a product of many probabilities, and thus the absolute values may be of little meaning. To alleviate this issue, we will further define a scaled version of the feature importance which will take value from 0 to 1:

$$\phi_j = \frac{\psi_j - \min_k(\psi_k)}{\max_k(\psi_k) - \min_k(\psi_k)}.$$
(3.19)

4 Experiments

In this section, we motivate the use of sparsity to compress our models. Experiments 1 to 3 are dedicated to the aforementioned feature selection strategies. Through a comprehensive set of simulation settings, we test our method to combine individual weight relevances into a measure of feature relevance and illustrate the feature selection algorithm based on this measure. These experiments provide significant evidence that removing unnecessary elements from the model greatly enhances its generalizability. Experiments 4 to 9 provide evidence for the efficacy of the weight pruning strategy. In Experiment 4, we demonstrate that we can retain the predictive power of a trained network while significantly reducing its complexity by pruning unnecessary weights, thus making the network much lighter. Building on this, Experiment 5 extends the pruning methods to real-world regression datasets, following the experimental setup outlined by Hernandez-Lobato and Adams (2015). Our results across ten datasets show that the full model achieves comparable or better errors in all cases, with the pruned model (50% reduction) often performing comparably or better than other methods. However, some datasets highlight the importance of a larger model size. In Experiments 6 and 7, we

demonstrate application on computer vision tasks. We extend comparison with experiments ran in Bayes by Backprop (BbB) on the MNIST and the CIFAR-10 datasets (Blundell et al., 2015; Krizhevsky and Hinton, 2009), showing that our method incurs a significantly lower accuracy drop under extreme pruning conditions. Experiment 8 extends our method's application to Convolutional Neural Networks, where it performs on par with competing approaches, surpassing the Horseshoe method in some cases (Louizos et al., 2017). Finally, in Experiment 9, we demonstrate the scalability of our method on a large VGG-like network (Zagoruyko, 2015), achieving comparable or better error rates with significantly higher sparsity compared to the Horseshoe methods (Louizos et al., 2017).

4.1 Experiments on Simulated Datasets

Experiment 1: Checking Relationship Between Influence and ψ

First, let us consider the simplest situation. We have a two-variable linear model to test how the estimated feature relevance varies when the actual relevance of the features is varied.

We generate n=2000 copies of $X_1,X_2,\epsilon \stackrel{iid}{\sim} N(0,1)$ and define

$$y_i = (1 - \alpha)x_{i1} + \alpha x_{i2} + \epsilon_i,$$

where $\alpha = \{0, 0.05, \dots, 1\}$. We fit a two-hidden-layer BNN with 20 and 10 hidden nodes.

Once we have the fitted model, the predicted relative contributions of X_1, X_2 can be obtained by finding ψ_1, ψ_2 according to (3.18). To provide validity to our measures, we compare the predicted relative feature importances, to the actual relative contribution of X_2 on Y. This is denoted by I, and defined as

$$I = 1 - \frac{\sum (y_i - \alpha x_{i2})^2}{\sum y_i^2}.$$

I is chosen as a scale-free measure of the actual feature relevance. As we move α from 0 to 1, we make X_2 more relevant than X_1 – as a result, I also rises from 0 to 1. Since the objective of this experiment is to compare relative contributions, and the network is small enough, we chose to use ψ (3.18). However, moving forward, for more general cases, we shall only use ϕ (3.19) measures. We observe the relationship between I, ψ_1, ψ_2 in Fig. (1). Per expectation, I and ψ_2 share an almost linear increasing relationship, and I and ψ_1 share an almost linear decreasing relationship. Thus, we can be confident that our estimate of the relative feature importance is able to catch the relative influence that feature has well enough.

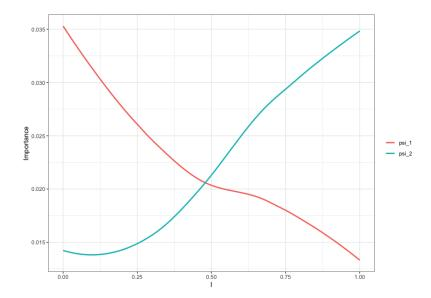


Figure 1: I vs ψ_1, ψ_2 (Experiment 1). As the importance of X_2 goes from 0 to 1, its estimated relevance goes up while the relative importance of X_1 goes down simultaneously.

Experiment 2: Generalizing for Many Input Features

We can further generalize Experiment 1 for many variables with more complicated data-generating functions and with varying effect sizes for each feature.

We generate n = 2000 copies of $X_1, X_2, \dots, X_D, \epsilon \stackrel{iid}{\sim} N(0, 1)$ and define

$$y_i = \sum_j f(X_{ij})\beta_j + \epsilon_i.$$

Here, $\beta_j = \frac{j}{\alpha}$, j = 1, 2, ..., D. The hyperparameters are as follows: D is the total number of features being used, α varies the overall level of signal-to-noise in the data by controlling β . We use several different $\alpha = \{1, 2, ..., 10\}$. And finally, f determines the relation between features and the response. We use two different such functions for illustration, one linear and one non-linear:

$$f(x) = x$$
, or $f(x) = e^{|x|} - 2x + \sin(2\pi x)$.

The purpose of this experiment is to inspect the correlation between ϕ_j and β_j with the understanding that the latter is a monotone function of the actual importance of the j^{th} feature and the former is an estimate of it. We observe the relationship in Figure

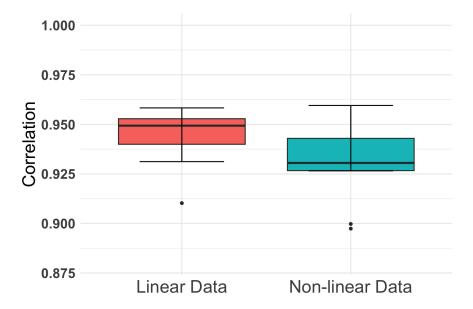


Figure 2: Correlation between Actual and Estimated Feature Importance. In all cases, correlations are high – however, the linear data-generating processes have lower variability.

2. We can verify the correlation is within the range (0.9, 0.95) for all datasets, which further strengthens our belief that the measure ϕ captures the relative distribution of the feature importance accurately enough. We also note that relationships are stronger and more stable in the case of linear data-generating models.

Typical Values of ϕ_j

Let us take this opportunity to discuss what the typical values of ϕ_j would look like. As mentioned earlier, using ψ_j directly might be problematic since it is a product of $p_i \in (0,1)$ and hence may become too small (e.g. for higher depth) to work with effectively. In contrast, ϕ_j represents the relative importance of each feature and is always valued between 0 and 1. Higher values of ϕ_j indicate greater influence of the feature.

Figure 3 illustrates two cases from this experiment. We are still operating in the non-linear data regime described by:

$$y_i = \sum_j f(X_{ij})\beta_j + \epsilon_i$$

where $\beta_j = \frac{j}{\alpha}$. As shown in Figure 2, ϕ_j aligns well with the relative contribution of

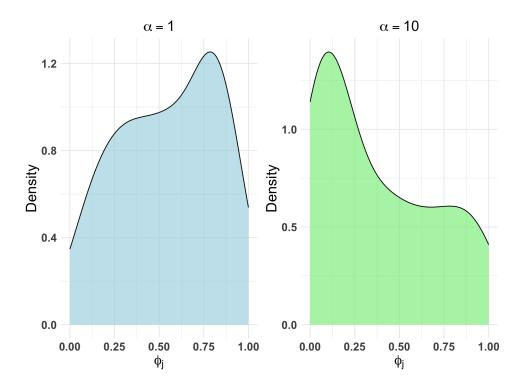


Figure 3: Correlation between Actual and Estimated Feature Importance. In all cases, correlations are high – however, the linear data-generating processes have lower variability.

each feature β_j through correlation analysis. Furthermore, for any fixed j, a higher value of α corresponds to a lower signal-to-noise ratio, leading to less influence. This effect is observable in Figure 3: for smaller α , the density of ϕ_j is left-skewed, indicating a greater number of features with high influence. Conversely, for larger α , the density is right-skewed, suggesting that fewer features have a high influence.

This behavior will be leveraged in the next section, where we will use ϕ_j to select a smaller set of active features by dropping less significant ones.

Experiment 3: Checking Prediction Power

Previous experiments provide ample evidence in support of the statement that our estimated feature relevance can efficiently capture the relative feature importance structure inherent in the dataset, even for complex data-generating processes. We will use this fact to do feature selection and demonstrate that the prediction power is improved by

using a smaller BNN instead of a more complicated one. We will also use several other models for baseline comparisons.

Every dataset in consideration will have n=2000 observations. Of which 80% are used for training and the rest for testing. Each dataset will consist of D features $X_1, X_2, ..., X_D \stackrel{iid}{\sim} N(0,1)$. Associated with every feature is a sparsity indicator $Z_1, Z_2, ..., Z_D \stackrel{iid}{\sim} \text{Bernoulli}(\pi)$ and an effect size coefficient $\beta_j = \frac{j}{\alpha}$. The response variable Y is generated as follows with $\epsilon_i \stackrel{iid}{\sim} N(0,1)$:

$$y_i = \sum_j f(X_{ij})\beta_j Z_j + \epsilon_i. \tag{4.1}$$

The hyperparameters of these experiments are α , f, D, π . The new and most important one among these is the sparsity hyperparameter π . This dictates what proportion of the features are actually active via determining how many Z_i s will be non-zero in any dataset. Rest are as defined in Experiment 2

The focal part of this experiment is testing the predictive and selective power of the feature selection method. For every dataset, we fit a BNN using our objective function. Based on the trained parameters, we determine the relative contribution of each feature according to (3.18). Then we make a smaller model by only keeping the 'important' features in the model and discarding the rest. Determining whether to keep a feature or not is done based on a threshold. Initially, we show the use of a fixed 80% quartile threshold, i.e. we only keep features with top 20% feature relevance. Later on, we will demonstrate the shortcomings of this method and how to find a dynamic threshold by employing cross-validation. The formal process is as follows:

Algorithm 2 BNN with Variable Selection (BNN_{VS})

```
1: function VS(\mathbf{P} = \{P_1, ..., P_L\})
2: Convert: P \to \phi_j \quad \forall \quad j = 1, 2, ... D
3: Compute: r = 80^{th} %-ile of the \phi_j
4: \hat{Z}_j = \mathbb{I}(\phi_j \geq r)
5: \mathcal{W}^T = (W_1, W_2, ..., W_D)
6: return \mathcal{W}
7: end function

8: function FIT(y, \mathbf{X}, \mathcal{W})
9: \mathbf{X}_{vs} = \mathbf{X} \cdot diag(\mathcal{W})
10: Train: BNN y \sim g(\mathbf{X}_{vs})
11: end function
```

The quantity \hat{Z}_j for each feature is of utmost interest. This denotes the inclusion of any feature in our smaller model. Ideally, this will be identical to Z_j for every feature. We can obtain the selection accuracy of the method for each dataset by verifying this

relationship $Acc. = \frac{1}{D} \sum_{1}^{D} \mathbb{I}(Z_j = \hat{Z}_j)$ We also measure whether discarding inactive features provide us with better generalization by comparing train and test MSEs in each of the datasets. We compare the improvement of generalizability of our method with the same obtained from the following baseline algorithms, NN (Unrestricted Neural Network), NN_{Dr} (Neural Network with Dropout), LM (Linear Model), BNN (Simple BNN) All of the Neural Networks are trained on a 2 hidden layer architecture with 20, and 10 hidden nodes respectively. We vary the hyperparameters α, f, π, D to generate different datasets and compare outputs in Figures (4, 5, 6).

Firstly, note that we use only top 20% features in the BNN_{VS} model, which means that our entire model is shrunk to 27% of its original size. However, Figures (4, 5) indicate that changing the effect size or the number of factors does not have any impact on the efficacy; we still get about a 90% accuracy in selecting the active features. Further, Figures 3, 4 also show the similarity between BNN_{VS} and NN_{Dr} methods, they both use shrinkage, in some form and thus demonstrate similar reductions in test errors in several scenarios that largely eclipse other methods. The other methods serve as a yardstick, we notice LM always has the highest training error and somewhat better test error showing underfit, while NN has the least training error and worst test error signaling clear signs of overfit.

Figure 5 shows a very interesting dynamic. Here we intentionally introduce misspecification. We vary the sparsity indicator from 0-95%, so each dataset has a different proportion of active features. But we only select top 20% of active features and discard the rest. We can notice that as the proportion of active features increases, the accuracy drops, as expected. BNN_{VS} still performs best in terms of test error as long as the proportion of active features increases is less than 50%(middle column), however, as we make more features active, the misspecification catches up $-BNN_{VS}$ show very high train as well as test error (rightmost column). Perhaps more interestingly, NN_{Dr} , which still takes all the features as input also suffers similarly.

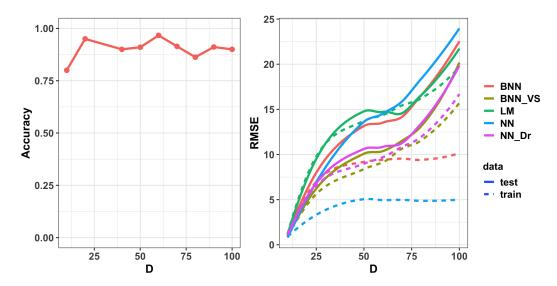


Figure 4: We vary D, the number of features. While keeping the following hyperparameters fixed: $\alpha = 2$, $f(x) = e^{|x|} - 2x + \sin(2\pi x)$, $\pi = 0.2$. We notice (Left) high selection accuracy and (Right)improved test errors in all such datasets.

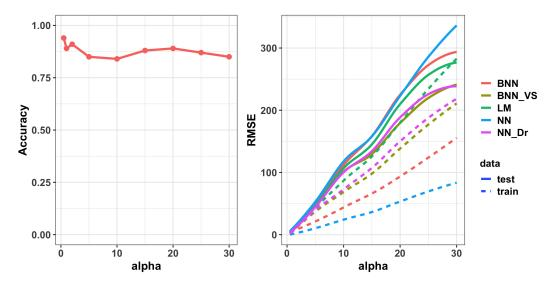


Figure 5: We vary α , the signal to noise ratio indicator. While keeping the following hyperparameters fixed fixed: $D=100, f(x)=e^{|x|}-2x+\sin(2\pi x), \pi=0.2$. We again notice (Left) high selection accuracy and (Right) improved test errors in all such datasets

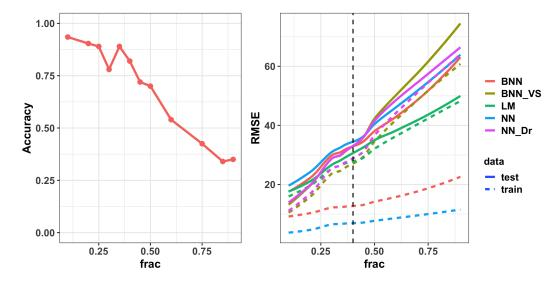
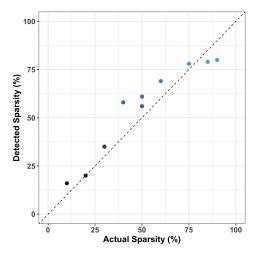
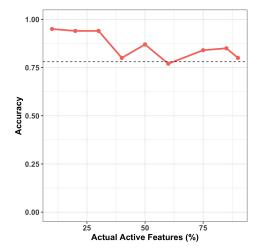


Figure 6: we vary the sparsity by varying π , while keeping the following hyperparameters fixed: D = 100, $f(x) = e^{|x|} - 2x + \sin(2\pi x)$, $\alpha = 2$. We notice (Left) a significant drop in accuracy and (Right) generalizability as more and more active features are ignored.

Cross Validation for Finding Optimal Thereshold

At this stage, we can employ cross-validation to understand what part of the input feature is indeed active. Let us focus on the data corresponding to Figure 6, we have 100 features, but the sparsity proportion is varying from 0-100% To automatically detect what proportion of the features are indeed active, we have implemented a 10-fold cross-validation setup. This dynamic threshold value obtained from CV can be used for feature selection instead of a pre-specified proportion. The results we find are insightful. If we repeat the experiments with varying proportions of active features, we can notice (Figure 7a) the estimated proportion of active features lines up relatively well with the actual proportion. More importantly, using this threshold now, we can select appropriate features (Figure 7b) – we observe that the accuracy of selecting relevant features never dips down, even though we do not know in advance what proportion of the features is actually active. Selecting correct features with high accuracy gives us better (Figure 8) test errors in almost all cases by some margin.





- (a) Actual Sparsity vs Detected Threshold. Points on and around y=x line indicate proper threshold detection.
- (b) Selection accuracy as the sparsity is varied. Accuracy never dips down and always stavs above 80%.

Figure 7: (a) We can detect feature selection threshold via CV. The actual proportions of active features align well with the detected proportions of active features. (b) Using such dynamically determined thresholds can help us find active features with high accuracy in any dataset with any given amount of sparsity.

Experiment 4: Weight Pruning in a Trained Network

For compressing an already trained neural network we can directly remove the weights that are not useful as determined by the final 'p' value obtained as an outcome of Algorithm 0. Since a higher value of 'p' indicates a stronger slab component and thus higher influence on the trained network. Using this strategy, we have the option to tune our level of compression based on our tolerance to error and the availability of resources. We demonstrate this again with the same data used in Experiment 3. If $\pi = 0.2$, i.e., only around 20% of the features are active, we can safely prune around 50 - 60% of the whole network and retain practically the same precision. Moreover, using simulation, we can notice that the volume of this 'sufficient' network changes when more features are active. If instead, we had $\pi = 0.5$, i.e. 50% of the features were actually active, we can only prune around 40% of the network before we start hemorrhaging precision. And when 90% of the features are active this number goes down to 20% - so about 80% of the model is useful. This phenomenon is illustrated in Figure 9.

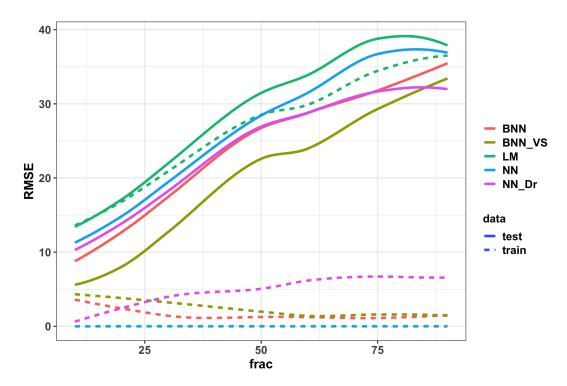


Figure 8: Capturing the correct features makes sure the smaller network almost always outperforms all other methods

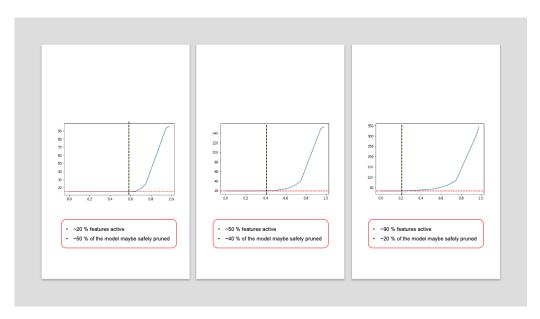


Figure 9: Weight Pruning in a Trained Network, (from left to right) more proportion of features are active. Thus, we will need to retain more proportion of the trained BNN to keep similar errors in test data.

4.2 Experiments on Regression Datasets

Experiment 5: Weight Pruning for Regression Analysis

In Section 4.1, we outlined the methodology for leveraging our algorithm's output to prune redundant weights from neural networks, resulting in significantly leaner networks while preserving their predictive capabilities. Extending this experiment to various real-world datasets, we align with the experimental setups described in Hernandez-Lobato and Adams (2015), Ghosh and Doshi-Velez (2017) by selecting ten publicly available datasets. The datasets are detailed in Table 1. Through regression analysis conducted on these standard datasets with standard architecture, we aim to demonstrate the efficacy of our approach.

Table 1: Dataset Characteristics

| Dataset | N | p |
|--|--------|----|
| Boston Housing (Harrison and Rubinfeld, 1978) | 506 | 13 |
| Concrete Compression Strength (Yeh, 2007) | 1030 | 8 |
| Energy Efficiency (Tsanas and Xifara, 2012) | 768 | 8 |
| kin8nm | 8192 | 8 |
| Naval Propulsion (Coraddu et al., 2014) | 11934 | 16 |
| Combined Cycle Power Plant (Tfekci and Kaya, 2014) | 9568 | 4 |
| Protein Structure (Rana, 2013) | 45730 | 9 |
| Wine Quality Red (Cortez et al., 2009) | 1599 | 11 |
| Yacht Hydrodynamics (Gerritsma et al., 2013) | 308 | 6 |
| Year Prediction MSD (Bertin-Mahieux, 2011) | 515345 | 90 |

The experimental setup maintains consistency with prior works, ensuring comparability with methodologies employed for comparison purposes. In this setup, each dataset undergoes a standard splitting procedure throughout our experiments into training and testing sets, with 90% of the data allocated for training and the remaining 10% for testing. The datasets are also normalized so that the input features and the response have zero mean and unit variance in the training set. The normalization on the response is omitted during prediction.

For training, we employed the Algorithm as described in section 3.2 on an 'oversized' neural network with one hidden layers consisting of 50 nodes each. However, for the year dataset, we augment the network with 100 hidden nodes. The performance evaluation metric utilized is the test root mean square error (RMSE) and the hyperparameters $\{\log \tau_1, \log \tau_0, \pi\}$ were set to $\{1, -6, 0.5\}$ respectively.

The resultant test RMSEs are summarized in Table 2. Here, Droprate denotes the proportion of removed weight. We examine how predictive performance changes as more and more weights are set to zero. The table unveils varying levels of redundancy within

the original network for different datasets. For example, certain datasets (e.g., wine) demonstrate the networks' ability to maintain predictive power even with nearly 90% of their weights pruned. In contrast, others (e.g., Power Plant, Protein) require the retention of most (more than 80%) of the network's weights to preserve comparable accuracy. This discrepancy is expected, reflecting the variability in the inherent complexity of the data generation processes.

This behavior is illustrated in Figure 10, which depicts the trajectory of test RMSE values as more unimportant weights are pruned. In most datasets, we observe consistent performance until approximately all but 50% of the weights are removed. However, for datasets such as Powerplant and Protein, the drop in performance occurs much earlier. We can further posit that employing a larger initial network would likely reveal higher levels of redundancy, as will be demonstrated in later experiments.

Table 2: Mean RMSE values for different datasets at varying Droprates

| DR (%) | Boston | Concrete | EnergyEff | Kin8nm | Naval | Powerplant | Protein | Wineqr | Yatch | Year |
|--------|--------|----------|-----------|--------|-------|------------|---------|--------|-------|-------|
| 0 | 3.07 | 5.54 | 0.69 | 0.08 | 0.00 | 4.00 | 4.48 | 0.62 | 0.94 | 8.75 |
| 10 | 3.07 | 5.54 | 0.69 | 0.08 | 0.00 | 4.00 | 4.52 | 0.62 | 0.94 | 8.76 |
| 20 | 3.07 | 5.54 | 0.69 | 0.09 | 0.01 | 4.26 | 4.78 | 0.62 | 0.94 | 8.76 |
| 25 | 3.07 | 5.54 | 0.69 | 0.16 | 0.01 | 5.28 | 4.80 | 0.62 | 0.94 | 8.76 |
| 50 | 3.07 | 5.54 | 0.69 | 0.33 | 0.01 | 8.77 | 4.84 | 0.62 | 0.94 | 8.76 |
| 75 | 3.69 | 16.39 | 0.72 | 0.33 | 0.02 | 16.74 | 5.05 | 0.73 | 1.01 | 10.26 |
| 80 | 4.03 | 17.09 | 1.06 | 0.31 | 0.03 | 17.07 | 6.33 | 0.78 | 1.17 | 10.39 |
| 90 | 6.22 | 14.98 | 6.15 | 0.27 | 0.04 | 17.08 | 11.15 | 0.79 | 4.27 | 11.35 |
| 95 | 7.18 | 15.03 | 10.08 | 0.26 | 0.03 | 17.08 | 7.69 | 0.79 | 7.94 | 11.33 |

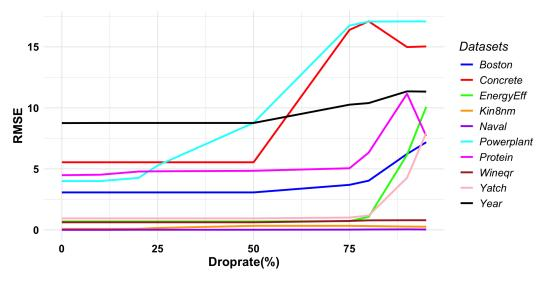


Figure 10

Next, we will assess the predictive efficacy of our model against some of the most prominent methods in the Bayesian Neural Network field that have demonstrated identical setups. Alongside the results for the full model (sBNN-50), we will also include results for the model with 50% of the weights pruned (sBNN-50). This will help us verify not only the efficacy of the model itself but also of the pruning process. We will compare these results with those from four comparable models. Probabilistic Backpropagation (PBP) (Hernandez-Lobato and Adams, 2015) serves as our baseline, this paper laid down the foundation for this experiment setup and along with Blundell et al. (2015); ? was among the pioneers of the modern implementation of the BNN. Additionally, we will include the Dropout (Gal and Ghahramani, 2016) method, as our method is intrinsically related to it and may be seen as a more generalized version of it. Further, we have added two more recent approaches that are closely related to our work, both of these employ some form of shrinkage prior. Horse-shoe BNN (HS-BNN) (Ghosh and Doshi-Velez, 2017) adopts a horseshoe prior and Sparse Variational BNN (SVBNN) (Bai et al., 2020) uses a different form of spike and slab prior (a mass at zero instead of a continuous spike prior). All the results are taken from their respective papers, the results for Bai et al. (2020) are taken from Liu and Wang (2024).

We find that the full model demonstrates competitive performance across all datasets, achieving the lowest mean RMSE in 7 out of 10 datasets. Among these, in Energy, Yacht, and Year, we observe substantial improvement over existing comparable methods. For the remaining three datasets, the error bars (computed as two standard errors from the mean value in each direction) overlap, indicating comparable results. Encouragingly, the model with a 50% reduction in load either outperforms or shows comparable performance to other methods in many datasets. However, exceptions are noted in the Power Plant, kin8nm, and Protein datasets, where the importance of having a larger model size becomes evident.

Table 3: Comparison of Different Methods on Various Datasets

| Dataset | sBNN | sBNN-50 | SVBNN | HS-BNN | Dropout | PBP |
|-------------|---------------------------------|---------------------------------|---------------------------------|-----------------|--------------------------------------|-----------------|
| Boston | 3.07 ± 0.14 | 3.07 ± 0.14 | 3.17 ± 0.58 | 3.32 ± 0.66 | $\mid \textbf{2.97}\pm\textbf{0.19}$ | 3.01 ± 0.18 |
| Concrete | 5.54 ± 0.14 | 5.54 ± 0.14 | 5.57 ± 0.47 | 5.66 ± 0.41 | $\textbf{5.23}\pm\textbf{0.12}$ | 5.67 ± 0.09 |
| Energy | $\textbf{0.69}\pm\textbf{0.08}$ | $\textbf{0.69}\pm\textbf{0.08}$ | 1.92 ± 0.19 | 1.99 ± 0.34 | 1.66 ± 0.04 | 1.80 ± 0.05 |
| Kin8nm | $\textbf{0.08}\pm\textbf{0.00}$ | 0.33 ± 0.02 | 0.09 ± 0.00 | 0.08 ± 0.00 | 0.10 ± 0.00 | 0.10 ± 0.00 |
| Naval | $\textbf{0.00}\pm\textbf{0.00}$ | 0.01 ± 0.00 | 0.00 ± 0.00 | 0.00 ± 0.00 | 0.01 ± 0.00 | 0.01 ± 0.00 |
| Power Plant | $\textbf{4.00}\pm\textbf{0.04}$ | 8.77 ± 0.49 | 4.01 ± 0.02 | 4.03 ± 0.15 | 4.02 ± 0.04 | 4.12 ± 0.04 |
| Protein | 4.48 ± 0.02 | 4.84 ± 0.02 | $\textbf{4.30}\pm\textbf{0.05}$ | 4.39 ± 0.04 | 4.36 ± 0.01 | 4.73 ± 0.01 |
| Wine | $\textbf{0.62}\pm\textbf{0.01}$ | $\textbf{0.62}\pm\textbf{0.01}$ | 0.62 ± 0.04 | 0.63 ± 0.04 | 0.62 ± 0.01 | 0.64 ± 0.01 |
| Yacht | $\textbf{0.94}\pm\textbf{0.06}$ | 0.94 ± 0.06 | 1.10 ± 0.27 | 1.58 ± 0.23 | 1.11 ± 0.09 | 1.02 ± 0.05 |
| Year | $8.75 \pm NA$ | $8.76 \pm NA$ | $8.87 \pm NA$ | 9.26 ± 0.00 | $8.85 \pm NA$ | $8.88 \pm NA$ |

4.3 Experiments on Image Classification Datasets Using Fully Connected Neural Networks

Experiment 6: Classification on MNIST

In this section, we apply our method to MNIST dataset in comparison with the experimental results of Section 5.1 from Blundell et al. (2015). To make fair comparisons, we used the same network structures and preprocessing procedure from Blundell et al. (2015). Specifically, we trained various networks of two hidden layers of rectified linear units and a softmax output layer with 10 units on the MNIST digits dataset, consisting of 60000 training and 10000 testing images. Each pixel of every image is divided by 126 before feeding to the network. For training, we ran SGD on our objective function for 300 epochs and considered learning rate of 0.05, 0.01 and 0.005 with minibatches of size 128. For hyperparameters tuning, we consider $\pi \in \{0.25, 0.5, 0.75\}$, $\log(\tau_1) = -1 + c$, $\log(\tau_0) = -5 - c$, where $c \in [0, 3]$, and perform binary search to determine c. Hyperparameters were chosen directly based on test accuracy, no validation set was considered. The chosen hyperparameters are reported in Table 4

Similar to other variational Bayesian frameworks, our objective function (3.6) is amenable to minibatch optimization, a strategy commonly used for neural networks. In every epoch of optimization, the training data \mathcal{D} is split randomly into a partition of M equally sized subsets, $\mathcal{D}_1, \dots, \mathcal{D}_M$. Each gradient is then averaged within one of these minibatches. Proposed by ?, a minibatch cost function can be defined by injecting one batch of data \mathcal{D}_i on the loss term while dividing the penalty term with M as follows,

$$\mathcal{J}_i(\theta) = -\mathbb{E}_{q(\mathbf{W})} \log p(\mathcal{D}_i|\mathbf{W}) + \frac{1}{M} \mathcal{R}(\theta). \tag{4.2}$$

such that $\sum_{i=1}^{M} \mathcal{J}_i(\theta) = \mathcal{J}(\theta)$. Minibatch cost function (4.2) evenly distribute the penalty across all minibatches. In this experiment, we use a different minibatch cost definition with non-uniformly distributed penalty suggested by Blundell et al. (2015) as follows,

$$\mathcal{J}_i(\theta) = -\mathbb{E}_{q(\mathbf{W})} \log p(\mathcal{D}_i|\mathbf{W}) + r_i \mathcal{R}(\theta)$$
(4.3)

where $\sum_{i=1}^{M} r_i = 1$. Blundell et al. (2015) suggests that minibatch cost (4.3) with schema $r_i = \frac{2^{M-i}}{2^M-1}$ works well. To put the comparison on equal footing, we used this same minibatch schema.

We start with comparing our result with Blundell et al. (2015) by reporting the test error. In Table 4, our method's classification error rate is comparable to that of the methods reported in Blundell's work.

Table 4: Classification Error Rates on MNIST

| Method | # Units/Layer | # Weights | Test Error | Hyperparameters |
|--------|--------------------|----------------------|------------|---|
| sBNN | 400 800 1200 | 500k 1.3m 2.4m | 1.47% | $ \begin{vmatrix} \pi = 0.5, \log(\tau_1) = 1.0, \log(\tau_0) = 0.002 \\ \pi = 0.5, \log(\tau_1) = 1.648, \log(\tau_0) = 0.002 \\ \pi = 0.5, \log(\tau_1) = 0.375, \log(\tau_0) = 0.007 \end{vmatrix} $ |

In Table 5, we examine the effect of replacing the variational posterior on some of the weights with a constant zero. We took the network with two layer of 1200 units trained in table 4, and order the weights by their posterior inclusion probability. We removed the weights with the lowest inclusion probability. The model demonstrates strong performance even when 98% of its weights are removed. We also provide the corresponding results for the method proposed in Blundell et al. (2015). It is essential to emphasize that our primary goal is to compare different sparsity levels within the same method rather than comparing between different methods.

Applying the heuristic signal-to-noise approach used in Blundell et al. (2015), their model experiences a reduction in efficacy of 7.75% when 98% of the neurons are removed. In contrast, our model only experiences a 3.1% decrease in efficacy under the same conditions. This contrast is consistently observed in every other sparsity condition as well.

Table 5: Classification Errors after Weight Pruning

| Proportion Removed | # Weights | Test Error (sBNN) | Test Error (BbB) |
|--------------------|------------------|-------------------|------------------|
| 0% | 2.4m | 1.58% | 1.24% |
| 50% | $1.2 \mathrm{m}$ | 1.57% | 1.24% |
| 75% | 600k | 1.52% | 1.24% |
| 95% | 120k | 1.54% | 1.29% |
| 98% | 48k | 1.61% | 1.39% |

In Figure 11, we examine the distribution of posterior inclusion probability of the network in Table 5. Most of the posterior inclusion probabilities are concentrated around 1 or smaller than 0.25, there are more than 95% of weights that have a posterior inclusion probability less than 0.25.

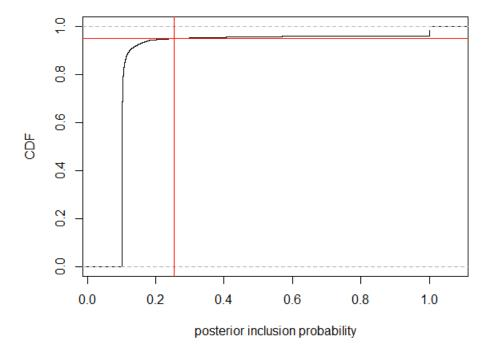


Figure 11: CDF of posterior inclusion probability over all weights in the network. The red line denotes the 95% cut-off.

Experiment 7: Classification on CIFAR-10

In their original paper, Blundell et al. (2015) only performed the aforementioned experiment with the MNIST dataset. Here, we extend the same methodology to the larger CIFAR-10 dataset. Unlike MNIST, CIFAR-10 is not greyscale; it consists of images with three color channels and dimensions of 32×32 pixels for each channel, with a 10-class classification output. For this experiment, we flatten all input pixels and train a two-hidden layer neural network, with each hidden layer containing 1200 nodes. Additionally, we train a model using BbB with the same architecture for comparison.

In summary, the results obtained from our experiments on the CIFAR-10 dataset reaffirm the efficacy of weight pruning techniques in reducing model complexity without significantly sacrificing classification performance. We observe a gradual increase in test error rates as the proportion of pruned weights increases, reflecting the loss of representational capacity in the model. However, even with significant weight pruning (e.g., 98% of weights removed), the performance degradation remains manageable, particularly considering the substantial reduction in model size and computational requirements.

Comparison with Blundell et al. (2015)'s method reveals similar trends to those observed in MNIST. The error rate in the original model is similar, and they remain comparable until 90% of weights are pruned. However, beyond that, our model shows greater robustness. For instance, under high pruning regimes, such as when 98% of the parameters are dropped, our model experiences a 29.3% drop in accuracy from the full model, whereas BbB suffers a drastic 66% drop. This example further emphasizes that if large pruning is the goal with spike and slab prior, the second moment of the weights (as in our method) is more appropriate than the signal-to-noise ratio (as in BbB). The details of this experiment are presented in table 6.

| Table 0. Classificati | Table 6. Classification Life after Weight I fulfing in Cliffit Dataset | | | | | |
|---|--|--------|--------|--|--|--|
| Proportion Removed # Weights Test Error (sBNN) Test Error (BbB) | | | | | | |
| 0% | 5.14m | 26.34% | 25.81% | | | |
| 50% | $2.57 \mathrm{m}$ | 27.02% | 25.86% | | | |
| 75% | 1.29k | 27.04% | 25.82% | | | |
| 90% | 514k | 26.63% | 26.26% | | | |
| 95% | 257k | 27.45% | 29.64% | | | |
| 98% | 103k | 33.92% | 42.83% | | | |

Table 6: Classification Errors after Weight Pruning in CIFAR10 Dataset

4.4 Experiments and Sparsity Comparison on Image Classification Datasets Involving Convolutional Layers

Experiment 8: Classification on MNIST using Lenet structures

In this segment, we further demonstrate the ability of our algorithm to induce sparsity in classification tasks and compare it with several widely used algorithms. For this purpose, as directed in Blalock et al. (2020), we will apply our method to train sparse neural networks on the MNIST dataset using a fully- connected architecture LeNet-300-100 and a convolutional architecture LeNet-5 (Lecun et al., 1998). These networks were trained from a random initialization and without data augmentation. We also extended our method to convolutional networks by associating all parameters from convolutional layers with spike and slab prior and learn the variational distribution in the exact same way we did for parameters in fully connected layer. During pruning phase, the cutoff threshold applies to variational inclusion probability of parameters from all convolutional layers and fully connected layers, so that sparsity also occur within the convolutional layer during pruning. Formally, we define sparsity using the following formula:

$$Sparsity = 1 - \frac{|w \neq 0|}{|w|},$$

where $|w \neq 0|$ denotes the count of non-zero weights and |w| represents the total number of weights in the network. Higher sparsity denotes a leaner network, goal is to achieve

a similar error range with as high sparsity as possible. This definition is similar to but not exactly same as the ones used in Louizos et al. (2017); Molchanov et al. (2017).

To contextualize our findings, we provide a comparative analysis, including error and sparsity metrics, against several state-of-the-art algorithms. These include Deep Compression (DC) (Han et al., 2015), Dynamic Network Surgery (DNS) (Guo et al., 2016) and Soft Weight Sharing (SWS) (Ullrich et al., 2017), Sparse Variational Dropout (SVD) (Molchanov et al., 2017), and Bayesian Compression using Group Horseshoe (BC-GHS) (Louizos et al., 2017). In Table 7, we can see our method performs head to head with all the competing approaches, beating the widely used horseshoe method in both tasks.

| Network | Method | Error % | Sparsity (%) |
|----------------|-------------------|---------|--------------|
| | Original | 1.64 | - |
| | DNS | 1.99 | 98.2 |
| Lenet-300-100 | SWS | 1.94 | 95.7 |
| Tellet-200-100 | Sparse VD | 1.92 | 98.5 |
| | DC | 1.59 | 92.0 |
| | BC-GHS | 1.80 | 89.4 |
| | sBNN (This paper) | 1.94 | 95.0 |
| | Original | 0.80 | - |
| | DNS | 0.91 | 99.1 |
| | SWS | 0.97 | 99.5 |
| Lenet-5-caffee | Sparse VD | 0.75 | 99.3 |
| | DC | 0.77 | 91.7 |
| | BC-GHS | 1.01 | 99.4 |
| | sBNN (This paper) | 1.06 | 99.2 |

Table 7: Comparison of Error % and Sparsity for different methods on Lenet architectures.

Discussion on Hyperparameter Tuning

In deep-learning architecture, hyperparameter tuning is a crucial aspect of optimizing model performance. Specifically, our setup involves three key hyperparameters: π (prior sparsity), τ_0 (slab prior standard deviation), and τ_1 (spike prior standard deviation). Initial experiments on smaller networks, as detailed in Section 4.2, indicated minimal discernible effects from these hyperparameters. However, a more extensive exploration in Section 4.4, which focuses on larger networks, reveals a more nuanced impact on both sparsity and test error.

In summary, when using two closely spaced values of $(\log \tau_1, \log \tau_0)$, we observe a relatively higher test error in the full network but the network retains substantial efficacy post-pruning. On the other hand, selecting more distant values for $(\log \tau_1, \log \tau_0)$ tends to yield a lower test error for the full network. However, this configuration may lead to a rapid loss of network efficacy after at a lower pruning level. Essentially, this denotes a trade-off between initial test error and the robustness of the network to pruning

Let us demonstrate this behavior in action with the Lenet5 architecture on MNIST. In the table below we exhibit some musings with two sets of values of the hyperparameters. In set 1, we used two values of $(\log \tau_1 = 0, \log \tau_0 = -5)$ that are relatively farther. While in set 2, we used two relatively closer values of $(\log \tau_1 = -1, \log \tau_0 = -3)$. Our analysis, as demonstrated in table 8 and figure 12, shows that the choice of (τ_1, τ_0) values significantly influences the performance of the network in achieving an optimal trade-off between test RMSE and network sparsity.

| Droprate | Test Error (Set 1) | Test Error (Set 2) |
|----------|--------------------|--------------------|
| 0.0 | 0.70 | 1.03 |
| 96.0 | 0.69 | 1.01 |
| 97.0 | 0.87 | 1.01 |
| 98.0 | 1.56 | 1.01 |
| 98.2 | 1.78 | 0.99 |
| 98.5 | 2.64 | 1.00 |
| 98.7 | 3.39 | 1.02 |
| 99.0 | 4.46 | 1.03 |
| 99.2 | 9.99 | 1.06 |
| 99.5 | 24.93 | 1.30 |
| 99.7 | 63.82 | 1.78 |
| 99.9 | 83.08 | 31.62 |

Table 8: Test Error for Different Droprates

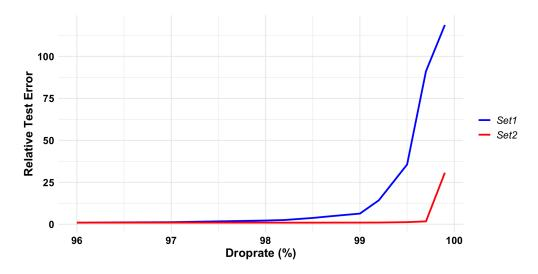


Figure 12: We demonstrate the proportional increase in test error in the two scenarios, considering pruning levels beyond 96%. Each line in the figure represents the test error at that level of pruning over the original test error for that model.

As we can see, the test error with the full network is quite low in Set 1 (0.7%). In fact, Set 1 achieves state-of-the-art error for this architecture with the full model but only maintains this performance up to 96% pruning. Beyond that, the error rate increases rapidly, making this pruning level less comparable to other methods in Table 7.

In Set 2, the full model's error might be slightly higher (1.03%), but more of the network can be pruned without significant efficacy loss. In this particular case, we can achieve 99.2% sparsity with a 1.06% test error, which is more comparable to methods such as BC-GHS (Louizos et al., 2017). This result is demonstrated in Table 7. Even beyond that, a 99.7% pruning retains an error rate of 1.78%, within a percentage point of the original result, which one might find acceptable. For Set 1, similar accuracy is only achieved around 98.2% sparsity and not beyond that. Figure 12 illustrates this robustness (or lack thereof) by showing the proportional increase in test error compared to the original network. As can be observed, the difference between the two models becomes noticeable around the 97% pruning stage and is highly significant when more than 98% of the respective networks are pruned.

These findings underscore the importance of tuning the appropriate values for τ_1 and τ_0 to achieve a delicate balance between overall error and sparsity metrics. One might prioritize a slightly higher potential test error with a smaller network or aim for a lower test error while preserving more of the original network. Ultimately, determining the optimal middle ground hinges on the user's sensitivity to the trade-off between error mitigation and resource utilization.

Experiment 9: Classification on CIFAR-10 with VGG-like structures

In this section, we demonstrate the scalability of our method to larger network structures by applying it to a VGG-like network (Zagoruyko, 2015) on the CIFAR-10 dataset (Krizhevsky and Hinton, 2009). The VGG network is a sizable mode. comprising 13 convolutional layers and two fully connected layers, with each layer followed by batch normalization. This architecture totals approximately 15 million parameters, a size that has proven imperative in breaking the 90% mark in test accuracy on CIFAR-10. However, such a large model is also ripe for pruning. We apply our pruning method to all weights in the convolutional and fully connected layers, removing all dropout layers from the architecture and using only our method for inducing sparsity.

Similar to the training and pruning strategy described in previous sections, we tuned our method's hyperparameters on a grid of values: $\pi \in \{0.25, 0.5, 0.75\}$, $\log(\tau_1) \in \{-6, -5, -4\}$, and $\log(\tau_0) \in \{-2, -1, 0\}$, and pruned the network based on the rank of variational inclusion probability. We trained our network with pre-trained weights and achieved a test accuracy of 91.4% with the hyperparameters set at $\pi = 0.5$, $\log(\tau_1) = 0$, and $\log(\tau_0) = -5$. Sparsity analysis showed that approximately 98.5% of the weights could be set to zero without significant change in accuracy.

As noted by Blalock et al. (2020), the VGG-like architecture is notorious for non-comparability among works. To provide a direct comparison, we utilized the two Horse-shoe Methods (Louizos et al., 2017) in table 9. Our approach achieves a better or equivalent error rate at a much higher level of sparsity compared to these methods.

| Network | Method | Error % | Sparsity (%) |
|----------|------------------------------|---------|--------------|
| | Original BC-GNJ BC-GHS | 7.6 | - 93.3 |
| VGG-like | BC-GN3 BC-GHS | 9.0 | 94.5 |
| | sBNN (This paper) | 8.7 | 98.5 |

Table 9: Comparison of Error % and Sparsity for different methods on VGG architectures on CIFAR-10 dataset.

5 Conclusion

In this work, we developed a novel strategy to incorporate Bayesian methods for sparsity detection into deep learning frameworks. By utilizing the inclusion probabilities from a Bayesian Neural Network (BNN), induced by applying a spike-and-slab prior, we can effectively identify sparsity within the model. This identified sparsity can then be leveraged to compress the model significantly, reducing its size while retaining its predictive power.

Several intriguing future directions arise from this work. One potential avenue is to use the order of sparsity obtained via inclusion probabilities p_i to hypothesize and determine the optimal architecture for the model, potentially leading to more efficient and tailored network designs. Additionally, exploring the theoretical guarantees of the feature selection methods we have proposed presents a rich area for further research. Understanding these guarantees could enhance the robustness and applicability of our methods.

We encourage practitioners in the Bayesian deep learning community to adopt this technique and *illuminate their black-boxes* by applying it to larger and more complex projects. This approach not only offers practical benefits in terms of model compression and interpretability but also contributes to advancing the field of Bayesian deep learning by providing clearer insights into model structure and feature importance.

S1: Proof for Proposition 3.1

Recall the objective function

$$\mathcal{J}(\theta, \mathbf{p}) = -\mathbb{E}_{q_{\theta}(\mathbf{W})} \mathbb{E}_{q_{\mathbf{p}}(\mathbf{Z})} \log \frac{p(\mathcal{D}|\mathbf{W}) \cdot \pi(\mathbf{W}, \mathbf{Z})}{q_{\theta}(\mathbf{W}) \cdot q_{\mathbf{p}}(\mathbf{Z})}$$
$$= -\mathbb{E}_{q_{\theta}(\mathbf{W})} \log p(\mathcal{D}|\mathbf{W}) - \mathbb{E}_{q_{\theta}(\mathbf{W})} \mathbb{E}_{q_{\mathbf{p}}(\mathbf{Z})} \log \frac{\pi(\mathbf{W}, \mathbf{Z})}{q_{\theta}(\mathbf{W}) \cdot q_{\mathbf{p}}(\mathbf{Z})}.$$

Write the second term as

$$(II) := \mathbb{E}_{q_{\theta}(\mathbf{W})} \mathbb{E}_{q_{\mathbf{p}}(\mathbf{Z})} \log \frac{\pi(\mathbf{W}, \mathbf{Z})}{q_{\theta}(\mathbf{W}) \cdot q_{\mathbf{p}}(\mathbf{Z})}$$
$$= \sum_{i} \mathbb{E}_{q_{\theta}(\mathbf{W})} \left(\mathbb{E}_{q_{\mathbf{p}}(\mathbf{Z})} \left(\log \pi(W_{i}, Z_{i}) - \log q(Z_{i}) \right) - \log q(W_{i}) \right).$$

Calculating these terms individually,

$$\begin{split} & \mathbb{E}_{q_{\mathbf{p}}(\mathbf{Z})} \left(\log \pi(W_i, Z_i) - \log q(Z_i) \right) \\ & = \mathbb{E}_{q_{\mathbf{p}}(\mathbf{Z})} \left(Z_i \left(\log \frac{\pi}{p_i} + \log N(w_i; 0, \tau_1^2) \right) + (1 - Z_i) \left(\log \frac{1 - \pi}{1 - p_i} + \log N(w_i; 0, \tau_0^2) \right) \right) \\ & = p_i \left(\log \frac{\pi}{p_i} + \log N(w_i; 0, \tau_1^2) \right) + (1 - p_i) \left(\log \frac{1 - \pi}{1 - p_i} + \log N(w_i; 0, \tau_0^2) \right). \end{split}$$

Thus,

(II) =
$$p_i \left(\log \frac{\pi}{p_i} + \mathbb{E}_{q_{\theta}(\mathbf{W})} \log \frac{N(w_i; 0, \tau_1^2)}{N(w; m_i, \sigma_i^2)} \right)$$

 $+ (1 - p_i) \left(\log \frac{1 - \pi}{1 - p_i} + \mathbb{E}_{q_{\theta}(\mathbf{W})} \log \frac{N(w_i; 0, \tau_0^2)}{N(w; m_i, \sigma_i^2)} \right).$ (A.1)

To simplify this, recall the following fact about Gaussian Distribution

$$\frac{N(X; a_1, b_1^2)}{N(X; a_2, b_2^2)} = \frac{b_2}{b_1} \exp \left\{ -\frac{1}{2} \left[\left(\frac{1}{b_1^2} - \frac{1}{b_2^2} \right) \left(X - \frac{\frac{a_1}{b_1^2} - \frac{a_2}{b_2^2}}{\frac{1}{b_1^2} - \frac{1}{b_2^2}} \right)^2 + \frac{(a_1 - a_2)^2}{b_1^2 - b_2^2} \right] \right\}.$$

Using this, we can check

$$\mathbb{E}_{q_{\theta}(\mathbf{W})} \log \frac{N(w_i; 0, \tau_1^2)}{N(w; m_i, \sigma_i^2)} = \log \frac{\sigma_i}{\tau_1} - \frac{m_i^2 + \sigma_i^2}{2\tau_1^2} + constant$$
 (A.2)

$$\mathbb{E}_{q_{\theta}(\mathbf{W})} \log \frac{N(w_i; 0, \tau_0^2)}{N(w; m_i, \sigma_i^2)} = \log \frac{\sigma_i}{\tau_0} - \frac{m_i^2 + \sigma_i^2}{2\tau_0^2} + constant.$$
 (A.3)

Using (A.1), (A.2), and (A.3), we get

$$\mathbb{E}_{q(\mathbf{W})} \mathbb{E}_{q(\mathbf{Z})} \log \frac{\pi(\mathbf{W}, \mathbf{Z})}{q(\mathbf{W}) \cdot q(\mathbf{Z})}$$

$$\begin{split} &= \sum_{i} \mathbb{E}_{q(\mathbf{W})} \left(\mathbb{E}_{q(\mathbf{Z})} \left(\log \pi(W_{i}, Z_{i}) - \log q(Z_{i}) \right) - \log q(W_{i}) \right) \\ &= \sum_{i} \left\{ p_{i} \left(\log \frac{\pi}{p_{i}} + \mathbb{E}_{q(\mathbf{W})} \log \frac{N(w_{i}; 0, \tau_{1}^{2})}{N(w; m_{i}, \sigma_{i}^{2})} \right) + (1 - p_{i}) \left(\log \frac{1 - \pi}{1 - p_{i}} + \mathbb{E}_{q(\mathbf{W})} \log \frac{N(w_{i}; 0, \tau_{0}^{2})}{N(w; m_{i}, \sigma_{i}^{2})} \right) \right\} \\ &= \sum_{i} \left\{ p_{i} \left(\log \frac{\pi}{p_{i}} + \log \frac{\sigma_{i}}{\tau_{1}} - \frac{m_{i}^{2} + \sigma_{i}^{2}}{2\tau_{1}^{2}} \right) + (1 - p_{i}) \left(\log \frac{1 - \pi}{1 - p_{i}} + \log \frac{\sigma_{i}}{\tau_{0}} - \frac{m_{i}^{2} + \sigma_{i}^{2}}{2\tau_{0}^{2}} \right) \right\} + constant \\ &= -\sum_{i} \mathcal{R}(\theta_{i}, p_{i}) + constant, \end{split}$$

which completes the proof.

S2: Proof for Proposition 3.2

The first term in $\mathcal{J}(\theta, \mathbf{p})$ is free of \mathbf{p} . Thus,

$$\frac{\partial \mathcal{J}(\theta, \mathbf{p})}{\partial p_i} = \frac{\partial \mathcal{R}(\theta, \mathbf{p})}{\partial p_i} = \left(\frac{m_i^2 + \sigma_i^2}{2\tau_1^2} - \frac{m_i^2 + \sigma_i^2}{2\tau_0^2}\right) + \left(\log \frac{\tau_1}{\pi} - \log \frac{\tau_0}{1 - \pi}\right) + \log \frac{p_i}{1 - p_i}.$$

So to optimize w.r.t p_i , we set:

$$\frac{\partial \mathcal{J}(\theta, \mathbf{p})}{\partial p_i} = 0$$

$$\implies \left(\frac{\tilde{m}_i^2 + \tilde{\sigma}_i^2}{2\tau_1^2} - \frac{\tilde{m}_i^2 + \tilde{\sigma}_i^2}{2\tau_0^2}\right) + \left(\log \frac{\tau_1}{\pi} - \log \frac{\tau_0}{1 - \pi}\right) + \log \frac{\tilde{p}_i}{1 - \tilde{p}_i} = 0$$

$$\implies \log \frac{\tilde{p}_i}{1 - \tilde{p}_i} = B_i - A_i$$

$$\implies \tilde{p}_i = \frac{1}{1 + \exp\{A_i - B_i\}}.$$

S3: Derivation in Section 3.3

The quantity of interest in \mathcal{J}_B (Blundell et al., 2015), is

$$f(W, m) = -\log \pi(W) + \log q(W|m).$$

Its gradient with respect to m can be found by using the reparametrization trick as outlined in Equation 3 in Section 3.2 of Blundell et al. (2015):

$$\nabla_{m} f = \frac{\partial f(W, m)}{\partial W} \frac{\partial W}{\partial m} + \frac{\partial f(W, m)}{\partial m}$$

$$= -\frac{\partial}{\partial W} \log \pi(W) + \frac{\partial}{\partial W} \log q(W|m) + \frac{\partial}{\partial m} \log q(W|m)$$

$$= -\frac{\partial}{\partial W} \log \pi(W),$$

where we use the facts that $W=m+\sigma\epsilon$ and therefore $\frac{\partial W}{\partial m}=1$, and the last equality is due to

$$\frac{\partial}{\partial m} \log q(W|m) = -\frac{(W-m)}{\sigma^2} = -\frac{\partial}{\partial W} \log q(W|m).$$

Hence

$$\nabla_m f = -\frac{\partial}{\partial W} \log \pi(W) = \left(\frac{W}{\tau_1^2} \frac{\pi_1(W)}{\pi(W)} + \frac{W}{\tau_0^2} \frac{\pi_0(W)}{\pi(W)} \right),$$

where we have used the notation: $\pi(W) = \pi_1(W) + \pi_0(W)$ and

$$\pi_1(W) = \pi \cdot N(W|0, \tau_1^2), \quad \pi_0(W) = (1 - \pi) \cdot N(W|0, \tau_0^2).$$

Next, we check the gradient with respect to σ^2 :

$$\nabla_{\sigma^{2}} f = \frac{\partial f(W, m)}{\partial W} \frac{\partial W}{\partial \sigma^{2}} + \frac{\partial f(W, m)}{\partial \sigma^{2}}$$

$$= \left(-\frac{\partial}{\partial W} \log \pi(W) + \frac{\partial}{\partial W} \log q(W) \right) \frac{\partial W}{\partial \sigma^{2}} + \frac{\partial}{\partial \sigma^{2}} \log q(W|\sigma^{2}).$$

Each term can be calculated and simplified to obtain:

$$\nabla_{\sigma^{2}} f = \left(\left(\frac{W}{\tau_{1}^{2}} \frac{\pi_{1}(W)}{\pi(W)} + \frac{W}{\tau_{0}^{2}} \frac{\pi_{0}(W)}{\pi(W)} \right) - \frac{W - m}{\sigma^{2}} \right) \frac{\epsilon}{2\sigma} - \left(\frac{1}{2\sigma^{2}} + \frac{\epsilon^{2}}{2\sigma^{2}} \right)$$

$$= \left(W \left(\frac{1}{\tau_{1}^{2}} \frac{\pi_{1}(W)}{\pi(W)} + \frac{1}{\tau_{0}^{2}} \frac{\pi_{0}(W)}{\pi(W)} - \frac{1}{\sigma^{2}} \right) + \frac{m}{\sigma^{2}} \right) \frac{\epsilon}{2\sigma} - \left(\frac{1}{2\sigma^{2}} + \frac{\epsilon^{2}}{2\sigma^{2}} \right)$$

$$= \frac{1}{2} \left(\frac{m}{\sigma} \epsilon + \epsilon^{2} \right) \left(\frac{1}{\tau_{1}^{2}} \frac{\pi_{1}(W)}{\pi(W)} + \frac{1}{\tau_{0}^{2}} \frac{\pi_{0}(W)}{\pi(W)} - \frac{1}{\sigma^{2}} \right) + \frac{1}{2\sigma^{2}} \left((\epsilon^{2} - 1) + \frac{m}{\sigma} \epsilon \right).$$

References

- Bai, J., Song, Q., and Cheng, G. (2020). "Efficient Variational Inference for Sparse Deep Learning with Theoretical Guarantee." 26
- Barber, D. and Bishop, C. (1998). "Ensemble Learning in Bayesian Neural Networks." In Generalization in Neural Networks and Machine Learning, 215–237. Springer Verlag. 4
- Bartoldson, B., Morcos, A., Barbu, A., and Erlebacher, G. (2020). "The generalization-stability tradeoff in neural network pruning." Advances in Neural Information Processing Systems, 33: 20852–20864. 1
- Belkin, M., Hsu, D., Ma, S., and Mandal, S. (2019). "Reconciling modern machine-learning practice and the classical bias-variance trade-off." *Proceedings of the National Academy of Sciences*, 116(32): 15849–15854. 1
- Bertin-Mahieux, T. (2011). "Year Prediction MSD." UCI Machine Learning Repository. DOI: https://doi.org/10.24432/C50K61. 24
- Blalock, D. W., Ortiz, J. J. G., Frankle, J., and Guttag, J. V. (2020). "What is the State of Neural Network Pruning?" In *Proceedings of Machine Learning and Systems* 2020, MLSys 2020, Austin, TX, USA, March 2-4, 2020. mlsys.org. 2, 30, 34
- Blundell, C., Cornebise, J., Kavukcuoglu, K., and Wierstra, D. (2015). "Weight Uncertainty in Neural Networks." In *Proceedings of the 32nd International Conference on International Conference on Machine Learning Volume 37*, ICML'15, 1613–1622. JMLR.org. 3, 4, 5, 6, 7, 10, 11, 12, 14, 26, 27, 28, 29, 30, 36
- Bykov, K., Höhne, M. M.-C., Creosteanu, A., Müller, K.-R., Klauschen, F., Nakajima, S., and Kloft, M. (2021). "Explaining bayesian neural networks." arXiv preprint arXiv:2108.10346.
- Casella, G. and Berger, R. (2002). Statistical Inference. Thomson Learning. 8
- Cheng, Y., Wang, D., Zhou, P., and Zhang, T. (2018). "Model Compression and Acceleration for Deep Neural Networks: The Principles, Progress, and Challenges." *IEEE Signal Processing Magazine*, 35(1): 126–136. 2
- Clyde, M., Desimone, H., and Parmigiani, G. (1996). "Prediction Via Orthogonalized Model Mixing." *Journal of the American Statistical Association*, 91(435): 1197–1208.
- Clyde, M. and George, E. I. (2004). "Model Uncertainty." Statistical Science, 19(1): 81 94. 2
- Collins, M. D. and Kohli, P. (2014). "Memory Bounded Deep Convolutional Networks." arXiv:1412.1442. 5
- Coraddu, A., Oneto, L., Ghio, A., Savio, S., Anguita, D., and Figari, M. (2014). "Condition Based Maintenance of Naval Propulsion Plants." UCI Machine Learning Repository. DOI: https://doi.org/10.24432/C5K31K. 24

- Cortez, P., Cerdeira, A., Almeida, F., Matos, T., and Reis, J. (2009). "Wine Quality." UCI Machine Learning Repository. DOI: https://doi.org/10.24432/C56S3T. 24
- Courbariaux, M., Hubara, I., Soudry, D., El-Yaniv, R., and Bengio, Y. (2016). "Binarized Neural Networks: Training Deep Neural Networks with Weights and Activations Constrained to +1 or -1." 6
- Dinh, V. C. and Ho, L. S. (2020). "Consistent feature selection for analytic deep neural networks." In Larochelle, H., Ranzato, M., Hadsell, R., Balcan, M., and Lin, H. (eds.), Advances in Neural Information Processing Systems, volume 33, 2420–2431. Curran Associates, Inc.
 - URL https://proceedings.neurips.cc/paper_files/paper/2020/file/1959eb9d5a0f7ebc58ebde81d5df400d-Paper.pdf 2
- Faming Liang, Q. L. and Zhou, L. (2018). "Bayesian Neural Networks for Selection of Drug Sensitive Genes." Journal of the American Statistical Association, 113(523): 955–972. PMID: 31354179.
- Gal, Y. (2016). "Uncertainty in Deep Learning." Ph.D. thesis, University of Cambridge.
- Gal, Y. and Ghahramani, Z. (2016). "Dropout as a Bayesian Approximation: Representing Model Uncertainty in Deep Learning." In Proceedings of the 33rd International Conference on International Conference on Machine Learning Volume 48, ICML'16, 1050–1059. JMLR.org. 6, 26
- George, E. I. and McCulloch, R. E. (1993). "Variable Selection via Gibbs Sampling." Journal of the American Statistical Association, 88(423): 881–889. 2
- (1997). "Approaches for Bayesian Variable Selection." *Statistica Sinica*, 7(2): 339–373. 2
- Gerritsma, J., Onnink, R., and Versluis, A. (2013). "Yacht Hydrodynamics." UCI Machine Learning Repository. DOI: https://doi.org/10.24432/C5XG7R. 24
- Ghosh, S. and Doshi-Velez, F. (2017). "Model Selection in Bayesian Neural Networks via Horseshoe Priors." 24, 26
- Goan, E. and Fookes, C. (2020). "Bayesian Neural Networks: An Introduction and Survey." In *Case Studies in Applied Bayesian Data Science*, 45–87. Springer. 4
- Goh, Y.-S. and Tan, E.-C. (1994). "Pruning Neural Networks During Training by Backpropagation." In *Proceedings of TENCON'94 1994 IEEE Region 10's 9th Annual International Conference on: 'Frontiers of Computer Technology'*, 805–808 vol.2. 2
- Goodfellow, I., Bengio, Y., and Courville, A. (2016). *Deep Learning*. MIT Press. http://www.deeplearningbook.org. 1
- Guo, Y., Yao, A., and Chen, Y. (2016). "Dynamic Network Surgery for Efficient DNNs." 31
- Han, S., Mao, H., and Dally, W. J. (2015). "Deep Compression: Compressing

- Deep Neural Networks with Pruning, Trained Quantization, and Huffman Coding." arXiv:1510.00149. 5, 31
- Harrison, D. and Rubinfeld, D. L. (1978). "Hedonic housing prices and the demand for clean air." *Journal of Environmental Economics and Management*, 5: 81–102. URL https://api.semanticscholar.org/CorpusID:55571328 24
- Hernandez-Lobato, J. M. and Adams, R. P. (2015). "Probabilistic backpropagation for scalable learning of Bayesian neural networks." In Proceedings of the 32nd International Conference on International Conference on Machine Learning - Volume 37, ICML'15, 1861–1869. JMLR.org. 13, 24, 26
- Hinton, G. E. and van Camp, D. (1993). "Keeping the Neural Networks Simple by Minimizing the Description Length of the Weights." In *Proceedings of the Sixth Annual Conference on Computational Learning Theory*, COLT '93, 5–13. New York, NY, USA: Association for Computing Machinery. 4
- Hoefler, T., Alistarh, D., Ben-Nun, T., Dryden, N., and Peste, A. (2021). "Sparsity in deep learning: Pruning and growth for efficient inference and training in neural networks." The Journal of Machine Learning Research, 22(1): 10882–11005. 1
- Hornik, K. (1991). "Approximation Capabilities of Multilayer Feedforward Networks." Neural Networks, 4(2): 251 – 257. 1
- Ishwaran, H. and Rao, J. S. (2005). "Spike and Slab Variable Selection: Frequentist and Bayesian Strategies." *The Annals of Statistics*, 33(2): 730–773. 2
- Janowsky, S. A. (1989). "Pruning versus Clipping in Neural Networks." *Physical Review* A, 39: 6600–6603. 2
- Kingma, D. P., Salimans, T., and Welling, M. (2015). "Variational Dropout and the Local Reparameterization Trick." In Advances in Neural Information Processing Systems, volume 28. Curran Associates, Inc. 6
- Kingma, D. P. and Welling, M. (2014). "Auto-Encoding Variational Bayes." In 2nd International Conference on Learning Representations, ICLR 2014, Banff, AB, Canada, April 14-16, 2014, Conference Track Proceedings. 5, 8
- Krizhevsky, A. and Hinton, G. (2009). "Learning Multiple Layers of Features from Tiny Images." 14, 33
- LeCun, Y., Bengio, Y., and Hinton, G. (2015). "Deep Learning." Nature, 521: 436–44.
- Lecun, Y., Bottou, L., Bengio, Y., and Haffner, P. (1998). "Gradient-based learning applied to document recognition." *Proceedings of the IEEE*, 86(11): 2278–2324. 30
- LeCun, Y., Denker, J. S., and Solla, S. A. (1990). "Optimal Brain Damage." In Advances in Neural Information Processing Systems, 598–605. Morgan Kaufmann. 5
- Li, Y., Chen, C.-Y., and Wasserman, W. W. (2015). "Deep Feature Selection: Theory and Application to Identify Enhancers and Promoters." In Przytycka, T. M. (ed.),

- Research in Computational Molecular Biology, 205–217. Cham: Springer International Publishing. 2
- Lindley, D. V. (1957). "A Statistical Paradox." Biometrika, 44(1-2): 187–192. 12
- Liu, J. (2021). "Variable Selection with Rigorous Uncertainty Quantification using Deep Bayesian Neural Networks: Posterior Concentration and Bernstein-von Mises Phenomenon." In Banerjee, A. and Fukumizu, K. (eds.), Proceedings of The 24th International Conference on Artificial Intelligence and Statistics, volume 130 of Proceedings of Machine Learning Research, 3124–3132. PMLR. 2
- Liu, Y. and Wang, X. (2024). "Implicit Generative Prior for Bayesian Neural Networks." 26
- Louizos, C., Ullrich, K., and Welling, M. (2017). "Bayesian Compression for Deep Learning." 4, 6, 14, 31, 33, 34
- MacKay, D. J. C. (1992). "A Practical Bayesian Framework for Backpropagation Networks." Neural Computation, 4(3): 448–472. 2, 4, 5
- Mitchell, T. J. and Beauchamp, J. J. (1988). "Bayesian Variable Selection in Linear Regression." Journal of the American Statistical Association, 83(404): 1023–1032.
- Molchanov, D., Ashukha, A., and Vetrov, D. (2017). "Variational Dropout Sparsifies Deep Neural Networks." In *International Conference on Machine Learning*, 2498–2507. PMLR. 6, 31
- Mozer, M. C. and Smolensky, P. (1988). "Skeletonization: A Technique for Trimming the Fat from a Network via Relevance Assessment." In *Proceedings of the 1st International Conference on Neural Information Processing Systems*, 107–115. Cambridge, MA, USA: MIT Press. 2
- Neal, R. M. (1995). "Bayesian Learning for Neural Networks." Ph.D. thesis, University of Toronto. 2, 4, 5
- O'Hara, R. B. and Sillanpää, M. J. (2009). "A Review of Bayesian Variable Selection Methods: What, How and Which." *Bayesian Analysis*, 4(1): 85 117. 2
- Olden, J. D., Joy, M. K., and Death, R. G. (2004). "An Accurate Comparison of Methods for Quantifying Variable Importance in Artificial Neural Networks using Simulated Data." *Ecological Modelling*, 3(178): 389–397. 13
- Rakin, A. S., He, Z., Yang, L., Wang, Y., Wang, L., and Fan, D. (2020). "Robust Sparse Regularization: Defending Adversarial Attacks Via Regularized Sparse Network." In *Proceedings of the 2020 on Great Lakes Symposium on VLSI*, GLSVLSI '20, 125–130. New York, NY, USA: Association for Computing Machinery. URL https://doi.org/10.1145/3386263.3407651 2
- Rana, P. (2013). "Physicochemical Properties of Protein Tertiary Structure." UCI Machine Learning Repository. DOI: https://doi.org/10.24432/C5QW3H. 24
- Rastegari, M., Ordonez, V., Redmon, J., and Farhadi, A. (2016). "XNOR-Net: ImageNet Classification Using Binary Convolutional Neural Networks." 6

- Rockova, V., Lesaffre, E., Luime, J., and Löwenberg, B. (2012). "Hierarchical Bayesian formulations for selecting variables in regression models." *Statistics in medicine*, 31(11-12): 1221–1237. 2
- Shayer, O., Levi, D., and Fetaya, E. (2018). "Learning Discrete Weights Using the Local Reparameterization Trick." In *International Conference on Learning Representations*.
- Smith, M. and Kohn, R. (1996). "Nonparametric Regression Using Bayesian Variable Selection." *Journal of Econometrics*, 75(2): 317–343. 2
- Srivastava, N., Hinton, G., Krizhevsky, A., Sutskever, I., and Salakhutdinov, R. (2014).
 "Dropout: A Simple Way to Prevent Neural Networks from Overfitting." J. Mach. Learn. Res., 15(1): 1929–1958.
 3, 5
- Ström, N. (1997). "Sparse Connection and Pruning in Large Dynamic Artificial Neural Networks." In Proceedings of 5th European Conference on Speech Communication and Technology (Eurospeech 1997), 2807–2810.
- Tfekci, P. and Kaya, H. (2014). "Combined Cycle Power Plant." UCI Machine Learning Repository. DOI: https://doi.org/10.24432/C5002N. 24
- Tokui, S. and sato, I. (2016). "Reparameterization trick for discrete variables." 6
- Tsanas, A. and Xifara, A. (2012). "Energy Efficiency." UCI Machine Learning Repository. DOI: https://doi.org/10.24432/C51307. 24
- Ullrich, K., Meeds, E., and Welling, M. (2017). "Soft Weight-Sharing for Neural Network Compression." 31
- Wang, S. and Manning, C. (2013). "Fast Dropout Training." In Proceedings of the 30th International Conference on Machine Learning, volume 28 of Proceedings of Machine Learning Research, 118–126. PMLR. 6
- Williams, R. J. (1992). "Simple Statistical Gradient-Following Algorithms for Connectionist Reinforcement Learning." *Machine Learning*, 8(3–4): 229–256. 5
- Yeh, I.-C. (2007). "Concrete Compressive Strength." UCI Machine Learning Repository. DOI: https://doi.org/10.24432/C5PK67. 24
- Zagoruyko, S. (2015). "92.45 on cifar-10 in torch." http://torch.ch/blog/2015/07/30/cifar.html. 14, 33
- Zhang, C., Bengio, S., Hardt, M., Recht, B., and Vinyals, O. (2021). "Understanding deep learning (still) requires rethinking generalization." Communications of the ACM, 64(3): 107–115. 1

Acknowledgments